A VERTICAL ACTIVE HANDREST TO AID IN DEXTEROUS TASKS AND TO PROVIDE GRAVITATIONAL SUPPORT

by

Charles Andrew Stewart

A thesis submitted to the faculty of
The University of Utah
in partial fulfillment of the requirements for the degree of

Master of Science

Department of Mechanical Engineering

The University of Utah

May 2012

STATEMENT OF THESIS APPROVAL

The thesis of Charles Andrew Stewart

has been approved by the following supervisory committee members:

William R. Provancher	, Chair	04/12/2012 Date Approved
Jake J. Abbott	, Member	01/04/2012 Date Approved
Donald S. Bloswick	, Member	01/04/2012 Date Approved

and by Timothy Ameel, Chair of

the Department of Mechanical Engineering

and by Charles A. Wight, Dean of The Graduate School.

ABSTRACT

Traditionally, hand rests are used to reduce muscle fatigue and to improve precision in small-workspace dexterous tasks. Dynamic hand rests have been shown to be beneficial for large-workspace planar tasks. However, providing high-bandwidth support in the vertical direction proves to be more challenging than in the horizontal plane. One must decouple the gravitational support of the arm from the intended vertical motion of the user. A vertically moving device, called the Vertical Active Handrest (VAHR), is presented in this thesis. This device dynamically supports the weight of the user's arm over a large workspace to add stability for precision dexterous tasks while providing gravitational support to the arm to reduce fatigue. The goal in developing the VAHR is to integrate its capabilities with the current Active Handrest, which provides dynamic support in the horizontal plane, thus creating a three degree-of-freedom active support device. The VAHR takes control inputs from a force sensor embedded in its armrest and from the tracked position of a tool. Studies were conducted with a variety of controllers and user input strategies to evaluate the VAHR's effectiveness at assisting participants in a single-axis tracking task. An initial pilot test with the VAHR shows no statistical improvements in tracking performance using force input control modes over conditions in which the arm is unsupported, or is supported by a static rest surface. The main experiment presented in this thesis focuses on either pure stylus position input or a

combination of position and force inputs. Tracking accuracy significantly improves compared to the unsupported condition while using stylus position input control. Poor performance under pure force control is attributed to the required activation of large muscle groups in the arm to provide force input to the VAHR's instrumented armrest. These large muscle groups are poorly suited for the agile tracking task used for experimentation. It is theorized that the better performance when using the stylus position control modes is because inputs from smaller, more dexterous muscle groups in the hand are utilized, allowing the position of the arm to be controlled by muscles that are already adept at precision control.

TABLE OF CONTENTS

ACKNOWLEDGMENTS

"Whatever you do, whether in word or deed, do it all in the name of the Lord Jesus, giving thanks to God the Father through him…work at it with all your heart, as working for the Lord, not for human masters, since you know that you will receive an inheritance from the Lord as a reward. It is the Lord Christ you are serving." Colossians 3:17-24.

First and Foremost I thank the Lord Jesus, for whom and through whom I do all things. I thank Him for giving me insight and knowledge, for filling me with joy during the longest most arduous times, and for surrounding me with many people who make my life rich.

I would like to thank my wonderful family. My wife Meagan has diligently supported and encouraged me during the process of writing this thesis, even to the point of skipping hours of sleep to stay up with me and cheer me on. My parents have supported me throughout my schooling, and without their steadfast love and encouragement I would not have gotten where I am today. There are too many other siblings, cousins, aunts, uncles, nieces, nephews and friends to mention who deserve many thanks for kind prayers and words of encouragement.

Special thanks go to Dr. William Provancher, my research advisor. With his guiding hand and wealth of knowledge I have learned far more in just a few years working in his lab than I ever did in a classroom setting. It was not until I began working in his lab as an undergraduate that I began to understand how to apply what my course work had taught

me to the real world, how to go from theoretical to actual. I am a better engineer and a better person for having been a part of his research group.

I would also like to thank my lab mates, who have been excellent coworkers and friends. Many thanks to Hamid who has been a partner in research for much of the work presented in this thesis.

Lastly, I would like to thank the National Science Foundation for their funding under award IIS-0746914, which made this research possible.

CHAPTER 1

INTRODUCTION

Completing tasks that require precision manipulation or holding a heavy tool for a long period of time can result in poor performance and fatigue in the forearm or upper arm. Traditionally, static surfaces have been used as hand and arm rests to aid with such tasks. The support provided by the surface helps to steady the arm and hand. For example, an artist uses a maulstick to provide wrist support when painting detailed images. Resting the arm and hand on a surface also helps reduce muscle fatigue [1]. The drawback to resting the arm on a static surface is that the workspace is limited to the range of motion of the wrist or intermittent repositioning of the arm is required.

Various passive repositionable devices have been developed to help overcome this limited workspace and to support the weight of the arm. The EZ Rest painting hand rest is an example of a nonpowered, repositionable device that takes the place of a maulstick [2]. Human-robot cooperative manipulators have also been used to support the arm against gravity and increase the dexterous workspace of the hand in applications that require precision hand motion. The Active Handrest (AHR) is an example of a device that assists with precision manipulations in the horizontal plane, increasing the dexterous workspace of the hand to a 25 by 25cm plane. The AHR uses a motorized two axis linear stage to reposition the surface supporting the users arm and hand. Presented in this thesis is the development and preliminary evaluation of the Vertical Active Handrest (VAHR),

a device that builds on the concept of the AHR, extending its workspace to include the vertical dimension. Figure 1.1 shows a user interacting with the current prototype of the device. Before integrating the concepts of the VAHR and the AHR to make a device capable of providing active support over a 3-DOF workspace it is necessary to understand the special requirements and challenges that arise from having the axis of motion of the handrest aligned with the gravitational load of the arm. As such, the goal in developing and testing the Vertical Active Handrest is to isolate the vertical axis and provide the arm with gravitational and ergonomic support to aid in dexterous tasks over a large vertical workspace similar to that achieved when moving the hand while keeping the elbow on a fixed rest. This device has a single degree-of-freedom along the vertical axis and tracks the desired motion of the user to provide support to the forearm/wrist. Potential applications of this and similar devices are to increase precision and reduce fatigue in dexterous tasks, assist persons with disabilities such as Cerebral Palsy or Spinal Muscular Atrophy in performing activities of daily living (ADL) such as eating and grooming, and aid in upper extremity rehabilitation [3, 4]. The current revision of the VAHR is designed to assist healthy persons in the completion of dexterous tasks and a vertical tracking task has been created to evaluate the VAHR's effectiveness. Optimization for rehabilitation or for assisting the disabled in the completion of ADL would require some redesign of the interface between the arm and the device and likely some modifications to the control algorithms.

The VAHR is capable of using multiple control input strategies. The velocity of the hand support can be set based on the force exerted by the user on the support, the position of the stylus/tool relative to the support, or a combination of force and stylus position. A

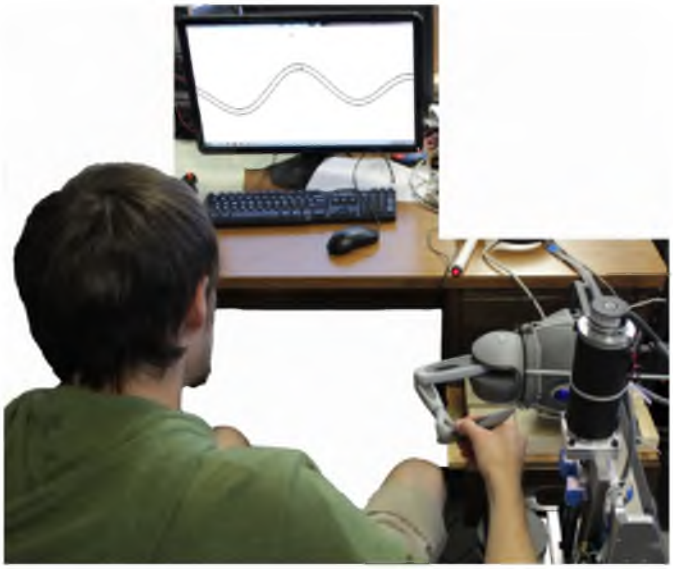

Figure 1.1 A test participant interacting with the VAHR

pilot study and an experiment were carried out in order to evaluate the VAHR's effectiveness under various control strategies to assist healthy persons in a one-dimensional vertical tracking task.

The three main contributions of this research are:

1. It is the initial step in extending the workspace of the planar Active Handrest to include the vertical dimension, the end goal being a three DOF assistive robotic device.
2. Experiment results show that the highest precision for controlling the VAHR is achieved when the small muscle groups of the wrist and hand, which are tuned for small scale precise motion, provide the control input rather than the large muscle groups of the shoulder and arm.
3. It shows that it is possible to achieve greater precision over a large workspace using an active, dynamic support than with a static support for the elbow, or with no support. This motivates future work on the VAHR.

1.1 Thesis Overview

There are six chapters to this thesis. The following is a brief summary of each chapter and its contribution to this thesis.

Chapter 1 gives an introduction to the project, describing the motivation behind creating and testing a single degree-of-freedom active dynamic arm support. The main contributions of this research are briefly summarized.

Chapter 2 provides a background on pertinent literature. The background focuses on three main fields of research: devices designed to cooperate with humans to provide fatigue reduction and/or increased precision, assistive devices for persons with upper extremity disabilities, and devices designed to facilitate upper extremity rehabilitation therapy.

Chapter 3 describes the design of the VAHR, including the goals in designing the VAHR, and a detailed description of the commercial components used in the prototype as well as the custom parts designed for the VAHR. The first prototype is described along with its important outcomes that influenced the design of the current prototype. Chapter 3 also discusses the configuration of the input device used in experimentation.

Chapter 4 describes the control architecture for the VAHR. Several control strategies, using different user input modes, for setting the desired velocity of the VAHR are described in detail.

Chapter 5 presents the experiment paradigm developed to evaluate the effectiveness of the various VAHR control modes, a vertical axis tracking task. Several other experiment paradigms that were considered are discussed briefly, and a detailed step-by-step description of how the paths for the tracking task were generated is given. The

general procedures followed during experimentation and the methods used to analyze experimental data are presented and the specific conditions tested in the pilot study, and in the initial experiment are given. Results for the pilot study and for the main experiment are presented, and some discussion concerning the implications of the results is given.

Chapter 6 provides conclusions to the thesis and presents the main contributions of this research. A summary of the ongoing work on the project is given, specifically, the motivation and design of a linkage that provides additional arm support. Several items of concern from the initial testing of the device that may need to be readdressed are presented as future work.

CHAPTER 2

BACKGROUND

The potential areas of application for the Vertical Active Handrest are to provide support to increase precision and reduce fatigue in dexterous tasks, to assist persons with upper extremity disabilities such as Cerebral Palsy or Spinal Muscular Atrophy in performing activities of daily living (ADL) and to aid in the rehabilitation of persons with upper extremity disorders. This chapter provides a brief background concerning various passive and active devices designed for each of these areas of application, including an overview of prior results with the planar AHR.

2.1 Assisting in Dexterous Tasks

The primary goals of designing a device that interfaces with the hand or arm for use in various dexterous tasks are to reduce muscle fatigue and to increase precision. Some devices are designed with only one of these two goals in mind, while others seek to satisfy both. In a combined research project the University of California and Lawrence Berkeley National Laboratory developed a three degree-of-freedom passive arm support with the goal of reducing muscle load for static and dynamic tasks [5]. This spring loaded support used torsion springs to provide a vertical support force to the forearms and succeeded in reducing muscle activity for tasks necessitating horizontal arm motions. However, the device was unsuccessful at lowering muscle load for tasks requiring

vertical arm motions, and is not conducive to rapid motions due to the device's high inertia. These limitations could potentially be overcome by an active arm support.

Human-robot cooperative manipulators have been used in applications that require precision hand motion. The "steady hand," a robotic system developed by Johns Hopkins University to help the user with submillimeter manipulation tasks, simultaneously takes force input from the user and from virtual environment constraints and moves the tool accordingly [6]. This device cooperatively controls the tool to add precision as the user performs a task, but it does not support the users arm to reduce fatigue.

A Cobot is another example of a device that collaborates with a human to manipulate an object, assisting the operator by constraining motion to a desired trajectory, necessitating foreknowledge of its environment or of the specific task [7]. In some regard Cobots can be considered passive devices, as they only use electro-mechanical actuation to steer nonholonomic joints to stay on a given trajectory. While these devices are helpful, they do not actively assist the user in moving the weight of the arm. Also, it is not always convenient to program a device for use in a specific environment or task.

In previous work in the Haptics and Embedded Mechatronics Lab at the University of Utah an "Active Handrest" (AHR) has been developed to assist with large workspace precision manipulation in the horizontal plane without prior knowledge of its environment [8]. The AHR extends the dexterous workspace of a hand to a 25 x 25 cm plane using a computer controlled, motorized two-axis stage to reposition the surface supporting the user's hand and arm. The desired velocity of the AHR is computed using an admittance control law that takes as an input either the force exerted on the hand

support, a virtual spring force computed as a function of the position of the stylus relative to a tare position, or a combination of these two.

2.1.1 AHR Experiment and Results

Initial Experiments on the AHR were carried out using a circle tracing task [8]. Each Participant used the stylus of a Phantom Omni held in his/her right hand to trace circles of various radii. Circles appeared on the computer screen one at a time in random locations within the workspace of the device. The three radii used were 7.5 mm, 40 mm, and 100 mm, where the latter was simply an arc spanning the workspace of the VAHR as a 100 mm circle would not fit within the workspace. Each participant traced four circles of each radius with each of four different support conditions: with a fixed wrist rest, with a fixed elbow rest, with the AHR, and unsupported. The tracing error and completion time were recorded for each circle to analyze performance for each support conditions. For the 40 and 100 mm radius circles the AHR significantly reduced the amount of tracing error compared to the other support conditions ($p < 0.001$). No significant improvement over the other support conditions was shown for the AHR for the 7.5 mm circle, which is likely because all points on this circle fell within the workspace of the wrist, making it unnecessary to reposition the hand while tracing this circle. Pooling the data for all three circle sizes and comparing the performance of the various support conditions showed that the AHR had a 36.6% reduction in tracing error over the unsupported case and a 26.0% reduction over using the best case fixed support (fixed wrist rest) [9].

2.2 Aiding Disabled Persons

There are multiple commercial devices available that aim to assist persons with upper extremity disabilities perform activities of daily living by providing gravitational support to one or both arms. These devices tend to be either entirely passive or contain a majority of passive (nonactuated) degrees-of-freedom; arm supports with multiple passive DOF and one active joint to raise and lower the arm are common. In general devices designed to assist persons with disabilities interface with the arm using a sling or cup designed to cradle much of the forearm and sometimes include an additional component to support the user's elbow. It is also common for these devices to have redundant rotational DOF in the horizontal plane to allow various arm positions and rotations. Some of these devices are intended for use in a specific task, such as eating, while others are designed to provide support over a given workspace to assist with many ADL.

The Armon Edero [10] is an example of a completely passive dynamic arm support, which, similar to the passive arm support presented by Odell et al. [5], uses a spring to support the weight of the user's arm. The tension in the spring can be adjusted by hand in increments, enabling the amount of support force to be varied. It is unlikely that someone with limited muscle function/strength would be able to adjust the amount of support force on his/her own, thus the user of this arm support would likely require assistance in order to adjust the support force for different tasks.

The Armon Ayura [10, 11] and the Dynamic Arm Support (DAS) [12] could be classified as devices with one or two semiactive DOF. Both, like the Armon Edero, use an adjustable spring system to provide arm support, but differ from the Edero in that the support force can be adjusted on the fly by the user via a remote. The remote for the

Ayura also allows the user to adjust the forward/backward tilt of the entire device and to lock the motion of certain joints depending on the requirements of the specific task. The Neater Arm Support (NAS) [13] is a semiactive device, differing from the two devices described above in that the arm brace is raised and lowered directly by a motorized mechanism. The motorized mechanism, and thus the vertical position of the arm, is controlled directly by the user with a remote. All three of these devices rely on remote controls for user input. This may necessitate the use of both hands to accomplish otherwise one handed tasks and may demand a higher cognitive load than would regularly be associated with a given task. Also, these devices do not make it possible for the user to control their velocity (in the case of the NAS) or the rate of change of arm support force (in the cases of the Ayura and the DAS).

2.3 Upper Extremity Rehabilitation

Arm rehabilitation therapy is used to help patients with hemiplegia or hemiparesis regain motor function. These conditions can result from a variety of ailments both congenital and acquired such as a stroke or cerebral palsy. It has been shown that repetitive task oriented motions, in which the arm is often constrained to some subset of its normal workspace, are an effective means of upper limb rehabilitation [14]. Conventionally in these techniques the arm of the patient would be supported and guided by a therapist; however, it is becoming more commonplace for patients to undergo therapy that is guided by passive arm supports or active rehabilitation robots. Robots are particularly well suited at administering rehabilitation therapy due to their aptitude at completing highly repetitive tasks and their ability to provide support forces and constraint forces to the arm.

It has been shown that poststroke patients can achieve greater elbow extensions in the horizontal plane when the forearm is supported externally against gravity rather than by an abduction torque at the shoulder [15]. Beer et al. suggest that providing scalable gravity compensation in arm rehabilitation may be beneficial, allowing variable rehabilitation intensity and gradual integration of support torques at the shoulder while extending the elbow [16]. A simple reaching task was designed in which the gravitational support force applied to the patient's arm was a function of arm position, specifically, support force increased with arm extension. In a preliminary study with five stroke patients they found that each participant's maximum reaching distance increased progressively as gravity compensation increased. [16]

Interactive rehabilitation robots often use computer control to provide assistance or resistance to patients navigating virtual environments. Sensors commonly measure joint and end effecter positions and interaction forces between the patient and the robot. This information is used in the various control strategies and in evaluating the recovery progress of patients. Motion can be constrained in some directions, and/or assisted in others depending on the goal of the therapy. The MIT Manus and the GENTLE/S are examples of rehabilitation robots that interface with a patient's wrist to guide the arm and hand along a predefined trajectory, both of which include a passive support for the elbow. The MIT Manus is an easily back drivable planar (two DOF) SCARA robot with an optional module that attaches to the end effector of the robot that has three additional active DOF for the wrist [17]. The joint torques of the robot are set using an impedance control strategy to give constant isotropic end effector stiffness and damping. The robot

provides assistance and guidance for patients who are otherwise unable to complete target motions.

The GENTLE/s is based on the Haptic Master, a three DOF commercial robot from FCS Robotics [18]. Attached to the end effector of the Haptic Master is a three DOF wrist support. The GENTLE/s uses one of three control modes with varying levels of assistance to guide patients along predetermined paths. The three control modes are labeled patient passive, patient active assisted, and patient active. In the patient passive mode the robot simply moves the patients arm to the target, and in the active assisted mode the robot guides and assists the patient's motion in the direction of the pathway according to the force he/she is applying to the end effector. In these two modes the motion of the robot along the predefined path is controlled to minimize jerk in order to approximate natural human motion. In the patient active mode the GENTLE/s remains passive until the patient deviates from the predefined path, in which case the robot employs a virtual spring damper system to pull the patient back onto the path. A "ratchet" function is also used in this mode such that backtracking along the path is not permitted.

CHAPTER 3

DEVICE DESIGN

The main goal in developing the Vertical Active Handrest is to provide active support to the arm for dexterous tasks, bearing the weight of the arm against gravity and expanding the precision workspace of the wrist and hand. The VAHR is limited to motion in a vertical axis in order to explore the special requirements of supporting the user's intended motion in an axis aligned with gravitational force. The VAHR must be capable of outputting high enough force to easily lift the weight of a typical arm. Its workspace should be similar to that achieved by raising and lowering the hand with the elbow resting on a fixed rest. The movement of the VAHR should be smooth throughout its workspace; there should not be any vibrations or oscillations perceptible to the user.

The Vertical Active Handrest consists of several main components. A single-axis linear motion stage is oriented vertically and is driven by a DC motor. A linear stage was chosen over other possibilities for providing locomotion (i.e., a robot arm) due to its simplicity and efficiency at constraining motion to a single, vertical axis. Mounted to the carriage of the linear motion stage is an assembly that includes a padded plate to support the user's forearm and hand. In order to control the VAHR it is necessary to measure the interaction force between the user and the support plate as well as the position of the support plate. A force sensor contained in the assembly that supports the arm measures the force exerted by the user on the support plate, and the position of the support is

obtained using an encoder attached to the motor shaft. One of the initial goals in developing a VAHR prototype was to determine the sufficiency of using the force sensor to both determine when the arm is lifted off the support plate as well as to sense the interaction force. The motion of the VAHR is controlled by a PC, using one of several possible input strategies, that reads the values from the force sensor and the encoder. An admittance control law is used to calculate a desired velocity and output commands to the stage's motor, adjusting the velocity of the support assembly to provide dynamic support to the user's arm.

3.1 Force Sensor Selection

Before designing the assembly to support the user's arm it was necessary to select an appropriate force sensor so that the assembly could be designed around the dimensions of this sensor. Several factors were considered in the selection of the force sensor that reads the users arm force. Upon measuring the weight of several people's arms resting on a digital scale, it was determined that an acceptable force sensor should have a range from approximately 0-45 N, the average weight of the entire human arm is 31.5 N [19]. In order to avoid mechanical failure in the event of user misuse (e.g., using the VAHR to support the weight of the body), however, it was decided that the force sensor should be able to support loads an order of magnitude higher than the typical weight of the arm without becoming unusable. Assuming that the force sensor should be able to support 25% of the user's body weight without damage, the sensor should be capable of withstanding loads greater than 160 N [19]. It was also important that the force sensor be accurate, providing a resolution small enough to detect minor adjustments in the force being applied by the user to the hand rest. A 222 N range minibeam load cell from

Omega (model #LCEB-50) with an ultimate overload capacity of 888 N was selected out of a list of four load cells that were considered to measure the force applied to the hand rest. This sensor was selected due to its high accuracy, low error (in terms of creep, linearity, hysteresis, and repeatability), high safe and ultimate overload capabilities, and its relatively low cost compared to some other force sensors. Table 3.1 shows a chart comparing the characteristics of the selected sensor with those of the other sensors that were considered.

3.2 Design of Force Sensor Housing

After the selection of the force sensor, the force sensor housing/support plate assembly was designed. Figure 3.1 shows a 3D model of the force sensor housing design, which consists of a 76.2 mm x 101.6 mm aluminum box-beam with a wall thickness of 6.35 mm supporting the force sensor.

Table 3.1 Force sensor selection comparison chart (data from [20])

	FULL-BRIDGE THIN-BEAM	OEM-STYLE SINGLE-POINT	STAINLESS STEEL COMPRESSION	MINIBEAM LOAD CELLS
Accuracy	0.25%	0.02%	0.50%	0.03%
Full Scale (N)	178	245	222	222
Price ($)	69 + 30	183	295	160
size (mm)	31.75 L x 7.925 W x 0.23 H	130 L x 40 W x 22 H	19 D x 12.7 H	60.5 L x 6.4 W x 25.7 H
form factor	rectangular	Beam	Cylinder	Mini beam
Input Voltage	5 (12 max)	10 (15 max)	5 (15 max)	10 (15 max)
Output	2mV/V	2mV/V	1mV/V	3mV/V
Safe Overload	150%	150%	150%	150%
Ultimate Overload		200%	300%	400%
Part Number	LCL-040	LCAE-25KG	LC302-50	LCEB-50

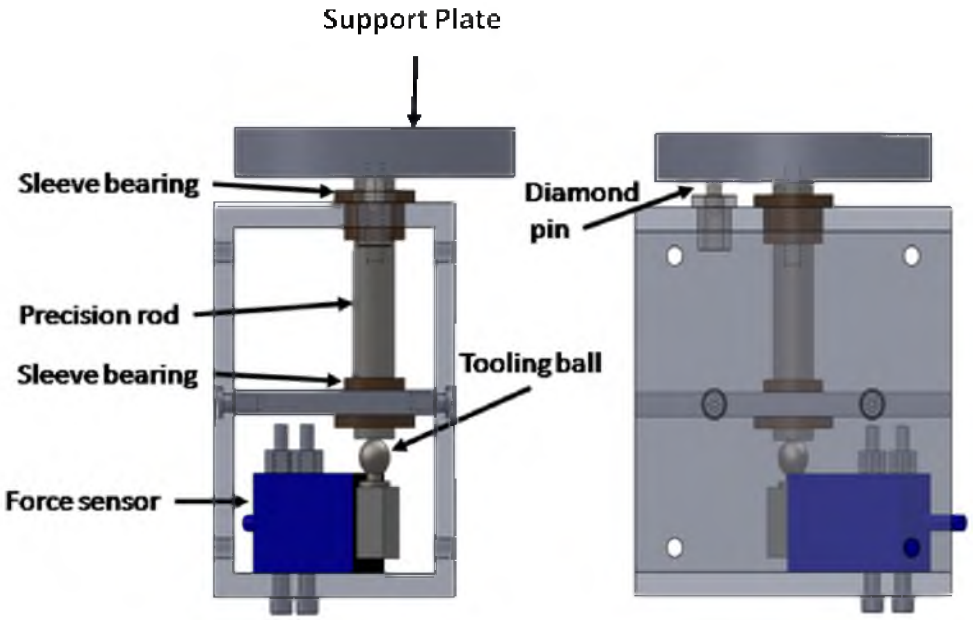

Figure 3.1 Force sensor housing with labeled components.

When operating the VAHR, the user's forearm rests on a circular, 12.7 mm thick support plate attached to a 12.7 mm diameter 316 stainless steel precision rod that transmits the user's vertical arm forces directly to the force sensor. A 13 mm thick foam rubber pad (not shown in Figure 3.1) is attached to the top of the support plate for comfort. A diamond shaped locating pin press fit into the underside of the support plate interfaces with a brass sleeve in the main housing to prevent the plate from rotating without hindering the transmission of force to the force sensor. In order to properly direct the vertical force the user applies to the support plate to the force sensor, while eliminating any cross-coupling from side loads that could possibly be applied to the support plate, two bronze sleeve bearings support the precision shaft while a tooling ball on the force sensor ensures point contact with the precision shaft. The two sleeve bearings and tooling ball eliminate off-axis loading from being transmitted to the force sensor, which would cause sensor bias.

As the force sensor's output is in the range of several millivolts an instrumentation amplifier chip (INA129) with a gain of 1000 amplifies the signal to a range of 0 to 10 volts before the signal is read by the Sensoray 626 card. The PCB housing the instrumentation amplifier also includes a low pass filter with a corner frequency of 40 Hz that reduces noise in the output signal.

To calibrate the force sensor, masses ranging of 0.1 to 11 Kg were placed on the hand rest plate. The output voltage from the instrumentation amplifier for each was recorded and a line was fit to the data predicting the amplified output voltage of the sensor given a specific force applied to it (Figure 3.2). The resulting calibration line fit the gathered data with a correlation coefficient (R^2) of 0.9994. The calibrated load cell had a sensitivity of 0.056 Volt/N.

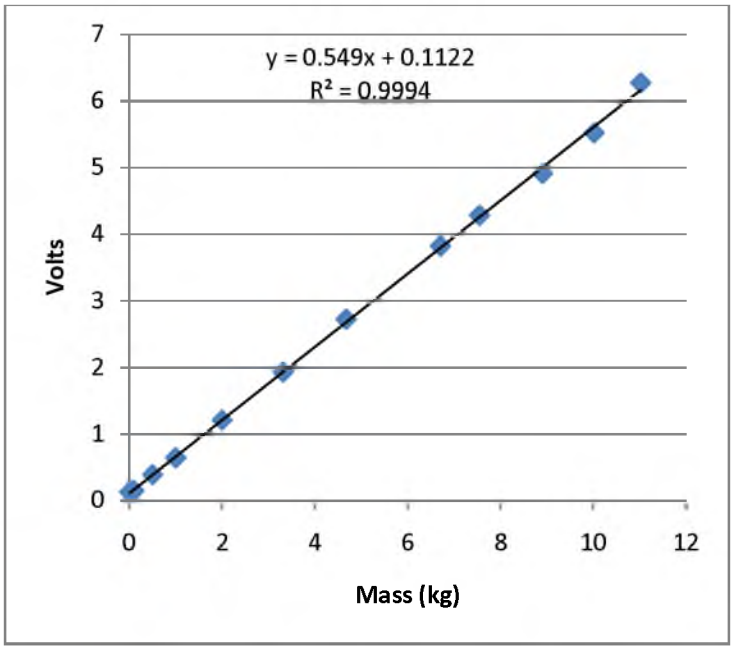

Figure 3.2 Force sensor calibration

In order to characterize the hysteresis in the force sensor assembly, the hand rest was loaded, unloaded and then the hand rest plate was lifted such that the rod transmitting forces to the load cell was no longer in contact with the force sensor input, next the rod was lowered slowly back onto the force sensor. The output force of the force sensor was recorded during this process and plotted versus time (Figure 3.3). The device was found to have 0.09 N of hysteresis due to the friction in the force sensor housing and to the hysteresis present in the force sensor itself. That is, there was a 0.09 N difference between unloaded conditions before and after the plate and rod were lifted off the force sensor and replaced. The amplified signal from the force sensor is passed through a low-pass filter in software with a corner frequency of 8.84 Hz to data reduce fluctuations of the input force to the controller and to counteract any high frequency noise in the force sensor signal.

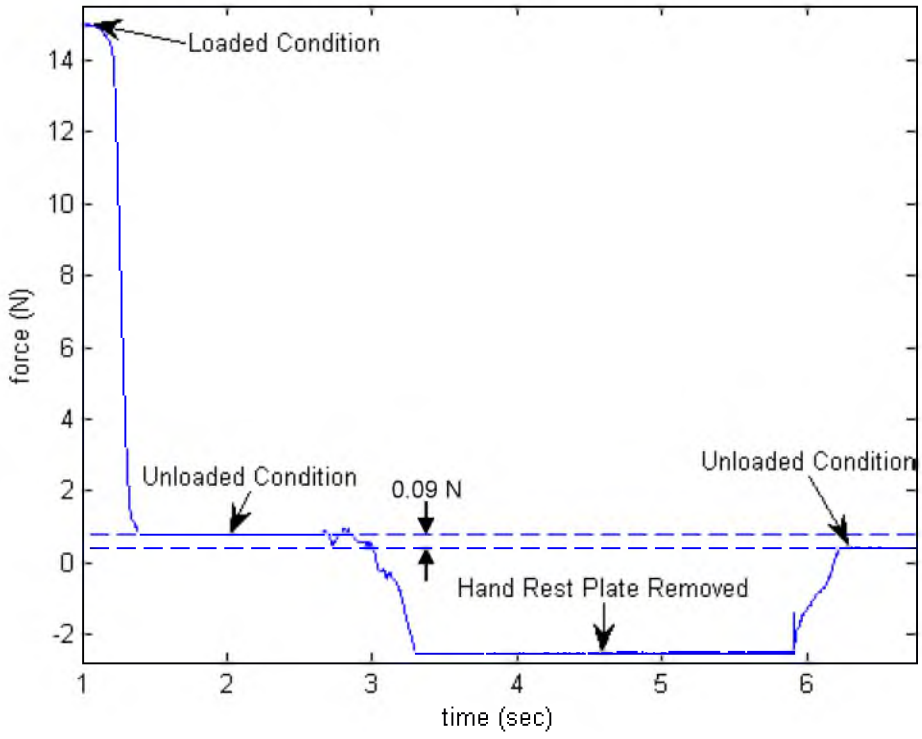

Figure 3.3 Hysteresis in the force sensor housing.

The typical weight test participants rested on the support plate ranged from 8.4 N to 24.5 N. During the tracking task, participants' force varied by approximately ±9 N from the neutral weight of the arm in order to control the movement of the stage (see chapter four for a description of the controller). The maximum force applied by a user to the support plate during experimentation was 63 N. Comparing these values to the 222 N range of the force sensor it appears that the sensor range is excessive for the forces it is measuring. It is possible, however, that participants applied much higher forces to the sensor during times in between experiment trials when no sensor readings were taken. Participants, for example, may have supported some of their body weight on the force sensor while readjusting their body position. One revision for a future VAHR prototype might be to replace the force sensor with one that has a range similar to the range of forces experienced during experimentation and to include some type of mechanical overload protection in the design of the force sensor housing. Use of an Omega mini-beam load cell with half the range (i.e., 111 N using an LCEB-25) would still provide a safe overload of 150% of the specified range and would safely handle the estimated 160 N applied to the force sensor when participants use the handrest to reposition themselves. This would also be well within the 400% ultimate overload capabilities specified by Omega for these force sensors [20]. An LCEB-10 (44.8 N) load cell would also be a possibility if mechanical overload protection was integrated into the design of the force sensor housing or wrist support. Reducing the range of the load cell could provide greater resolution in the range of forces applied to the support plate during normal VAHR operation.

3.3 Initial Prototype Design

The initial prototype of the Vertical Active Hand Rest, shown in Figure 3.4, utilized a modified belt driven single axis linear stage with a single sleeve bearing to direct the device along its guide rails (Figure 3.5). This stage was taken from a recycled incubator drawer positioned with a belt-driven axis of motion aligned vertically. As this stage was assembled and working, yet inexpensive it was a good candidate for the initial prototype as it could be readily modified without significant investment of time or cost.

A Maxon RE36 motor with a 4.8 to 1 gear ratio was used to drive the belt system and a HEDS 5540 encoder with 500 counts per revolution attached to the motor shaft provided position feedback. When operating in quadrature this encoder yielded a position resolution of 0.023 mm.

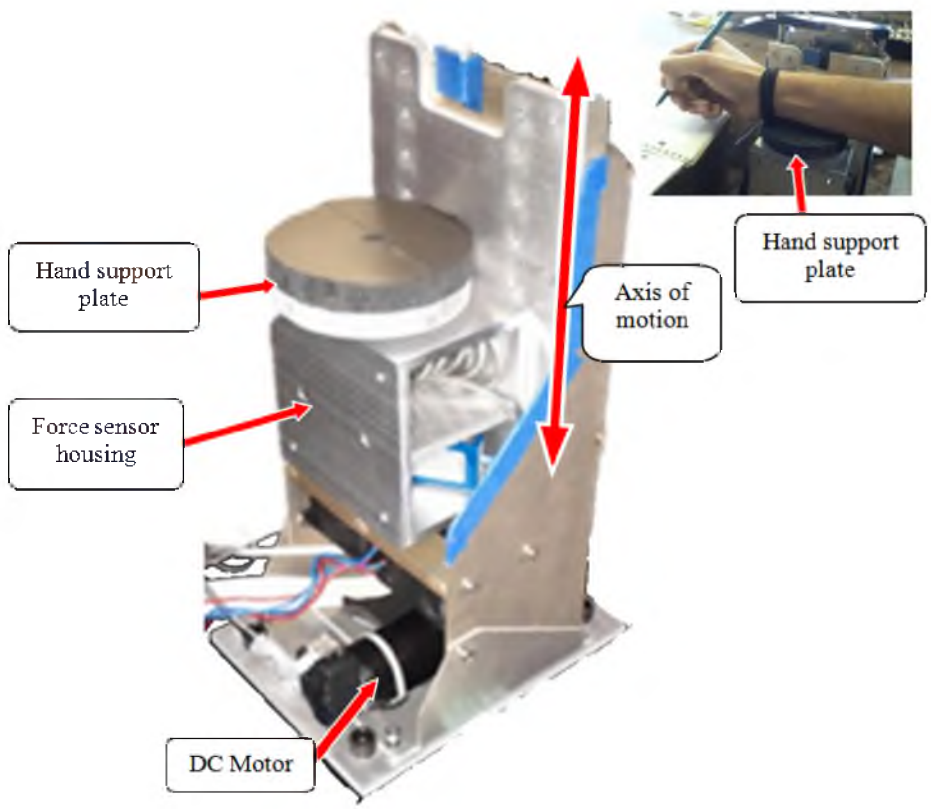

Figure 3.4 VAHR Initial prototype.

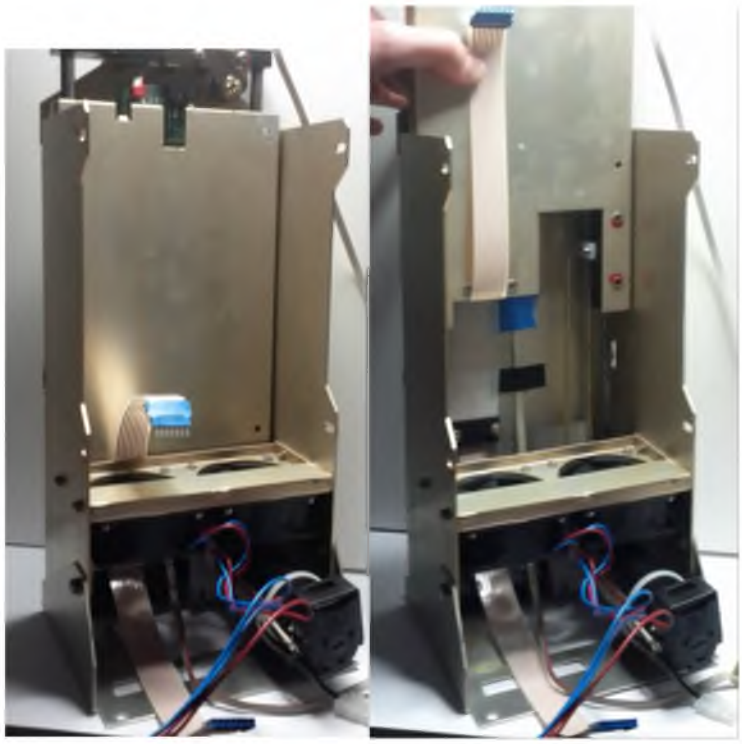

Figure 3.5 The initial prototype stage in its lowered (left) and raised (right) positions

A Sensoray Model 626 PCI Multifunction I/O Board measured amplified input forces from the user's arm. The digital-to-analog converter on the Sensoray 626 board output a voltage signal to an Advanced Motion Controls 12A8 Brush Type PWM Amplifier, which in turn drove the motor at a maximum of 2.5 Amps full scale. The voltage output from the 626 board was derived from the desired velocity of the stage, computed with an admittance control law (equation (4.1)) based on the force sensor reading (the control algorithm is presented in detail in Chapter 4). The linear stage was equipped with two optical limit switches to detect the limits of travel. In software the stage was limited to a workspace beginning 10 mm above the lower limit and 10 mm below the upper limit, giving a total range of motion of 190 mm.

3.4 Results and Conclusions from the Initial Prototype

The initial prototype of the VAHR was evaluated qualitatively for its effectiveness at providing support to the arm over its workspace and at stabilizing the hand for precision tasks. The initial prototype was ill-suited for running any formal experiments for two main reasons. Namely, the stage exhibited noticeable stick slip behavior and the force output capability was insufficient to reliably lift the user's arm. Despite these shortfalls several important results were obtained from evaluation of the initial prototype. Multiple naive users found that interacting with the VAHR was intuitive, the device following the users' intended motions. One goal of the prototype was to determine the sufficiency of using a single sensor to sense user input force and to determine when the arm is lifted off the support plate. Initial testing showed that a single force sensor is sufficient for detecting the presence of the forearm on the support plate and that no additional contact sensor is required. Additional information regarding the evaluation of the initial prototype is presented in the Appendix.

3.5 Second Prototype Stage and Motor Specifications

The linear stage selected for the redesign of the Vertical Active Handrest is a 305 mm travel low-profile single-axis linear stage with a 6.35 mm pitch, antibacklash lead screw assembly provided by Servo Systems (model LPS 12-20). This stage can handle a maximum dynamic load of 89 N which is much higher than the 20 N load that the initial prototype was capable of lifting, and is approximately twice as much as the largest arm weight support forces measured during the force sensor selection process. Moments of 10.98 N-m perpendicular to the lead screw axis can be supported safely. It is estimated that the largest moment arm that could be used to apply a perpendicular moment, given

the design of the force sensor housing, is roughly 125 mm; thus the largest safe load using this perpendicular moment calculation is 88N, which is similar to the maximum allowable dynamic load. The datasheet for the stage lists a maximum linear velocity of 380 mm/sec for a 12.7mm pitch lead screw [21]. Assuming that the interaction between the lead screw and the nut is the limiting factor on the maximum travel speed, it stands to reason that the maximum speed of the stage used for the VAHR (with a 6.35 mm pitch) is 190 mm/sec, half of 380 mm/sec. Experimentation showed that the stage begins to exhibit chatter at speeds over 120 mm/sec, slightly lower than the expected maximum translational velocity. The stage is driven by an Electrocraft RDM 103 brush type DC motor with a continuous stall torque of 0.388 N-m [22]. This translates to a continuous stall force output of the stage of approximately 311 N calculated using the following equation where 0.81 is the efficiency of the lead screw [21], l is the pitch and T_{stall} is the continuous stall torque.

$$F = 0.81\frac{2\pi T_{stall}}{l} \tag{3.1}$$

The stage is mounted vertically to an aluminum frame with the motor on the top end. The total height of the VAHR from the base of the frame to the top of the motor is 68 cm. The current prototype is shown in Figure 3.6. Attached to the motor shaft is an Accu-Coder 15T-01SF-1000N5DHV-F00 incremental encoder with 1000 counts per revolution providing approximately 2 μm resolution for position feedback, when operated in quadrature. The force sensor housing described in Section 3.2 is mounted to the moving carriage of the stage.

A Sensoray Model 626 PCI Multifunction I/O Board and an Advanced Motion Controls 12A8 Brush Type PWM current Amplifier are used, as described above, to read

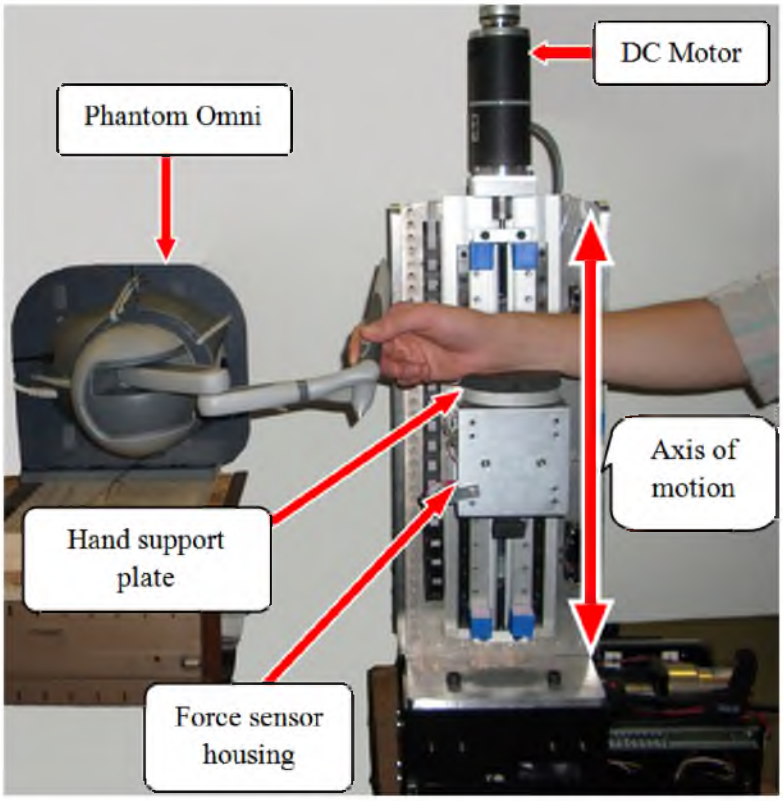

Figure 3.6 VAHR prototype with labels

force input and to drive the motor. The PWM amplifier is tuned to output a maximum of 5 Amps. The VAHR is mounted to an XY stage that has been disconnected from the lead screws, this makes repositioning the VAHR during experimentation easy.

3.6 Stylus Input

A SensAble Technologies Phantom Omni serves as an input device for experimentation, with test participants grasping the stylus of the Omni. We used Microsoft Visual Studio C++ and the Chai3D libraries [23] to interface with the Omni. Mounting the Omni on its side (as seen in Figure 3.7) achieves a greater vertical workspace as the Omni's horizontal workspace of 160 mm is greater than its vertical workspace of 120 mm. This modification better matches the workspace of the VAHR and

the requirements of the one-axis vertical tracking task used in evaluating the effectiveness of the VAHR. A custom PVC mounting bracket interfaces with rubber feet on the Omni and a yoke placed over the frame of the Omni pulls on and secures the Omni to the PVC bracket (Figure 3.7).

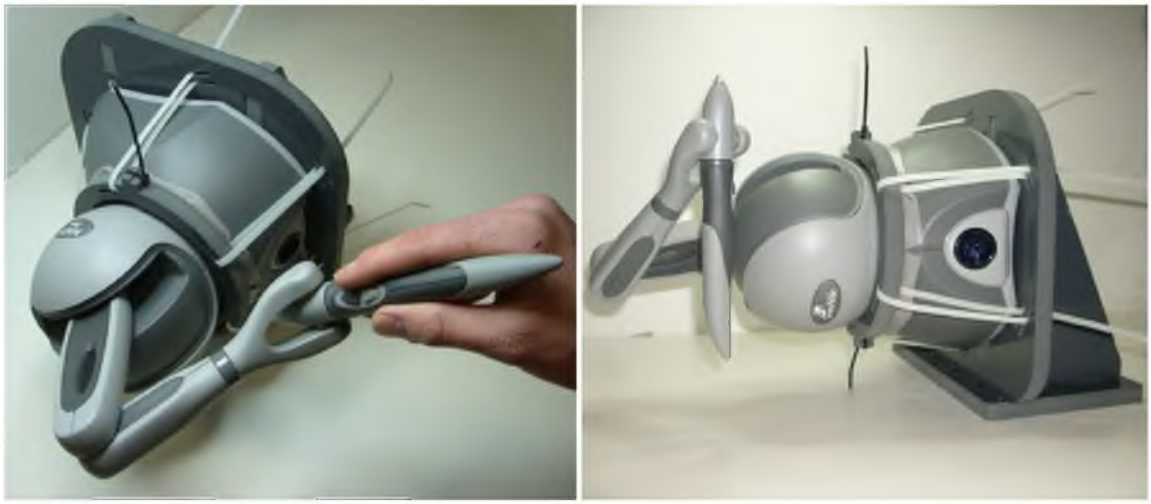

Figure 3.7 Phantom Omni mounted sideways on custom PVC bracket.

CHAPTER 4

CONTROLLER DESIGN

To control the motion of the VAHR an admittance control law is used to obtain a desired velocity of the stage based on the force applied to the support plate and the position of the stylus of the Phantom Omni. The desired velocity is numerically integrated to obtain a target position. A PID controller then sets the voltage output to the PWM current amplifier (AMC Model # 12A8) in order to drive the difference between the actual position of the Stage (obtained via reading the encoder on the motor) and the desired position to zero in order to provide dynamic support to the forearm.

4.1 Admittance Control Strategies

Several admittance-based control modes were investigated for setting the desired velocity of the VAHR. These control modes can be divided into three subcategories: force input, stylus input, and hybrid input. Each uses the measured "force" as an input to set the desired velocity of the vertical stage. The force input mode uses the force relative to the tared arm weight applied to the forearm support plate (measured by the force sensor) to set the desired velocity. The stylus input mode uses the position of the stylus relative to the position of the forearm support plate, and transforms this relative displacement into an input force using a virtual spring. The hybrid input mode uses an amalgamation of the arm rest force and the position of the stylus to set the desired

velocity. The desired velocity of the device is limited to ±110 mm/sec in all of these control modes. Also if the force applied to the support plate ever drops below 5% of the user's arm weight, it is assumed that the arm has been removed from the device and the desired velocity is set to zero. A control diagram for the hybrid input mode is shown in Figure 4.1. This figure is applicable to all the admittance control modes assuming that the contribution of the force sensor reading is zero for stylus input modes and that the contribution of the stylus position is zero for force input modes.

4.1.1 Force Input

Two force based admittance control laws are used: one that is proportional to the force applied to the support plate, and one that is proportional to the force squared. The force controllers tare the weight of the user's relaxed arm at the start of a session (and can retare manually as required). A dead band set around the tare value ensures that the stage velocity is maintained at zero unless the user changes their applied force to be outside of the dead band. Eqn. (4.1) shows the governing equation for the linear admittance controller:

$$V_{des} = K_a * (P_{db} * W_{arm} - F) \tag{4.1}$$

where V_{des} is the desired velocity, K_a is the admittance gain, W_{arm} is the weight of the user's arm while relaxed, F is the force measured by the force sensor and P_{db} is a proportion of W_{arm} that corresponds with the deadband. For upward motion, where $F < P_{db} * W_{arm}$, P_{db} is slightly less than one; for downward motion, where $F > P_{db} * W_{arm}$, P_{db} is slightly greater than one. We found via qualitative evaluation that setting different admittance gains for upward and downward motion that were also a function of arm weight made interaction with the VAHR feel more natural. The

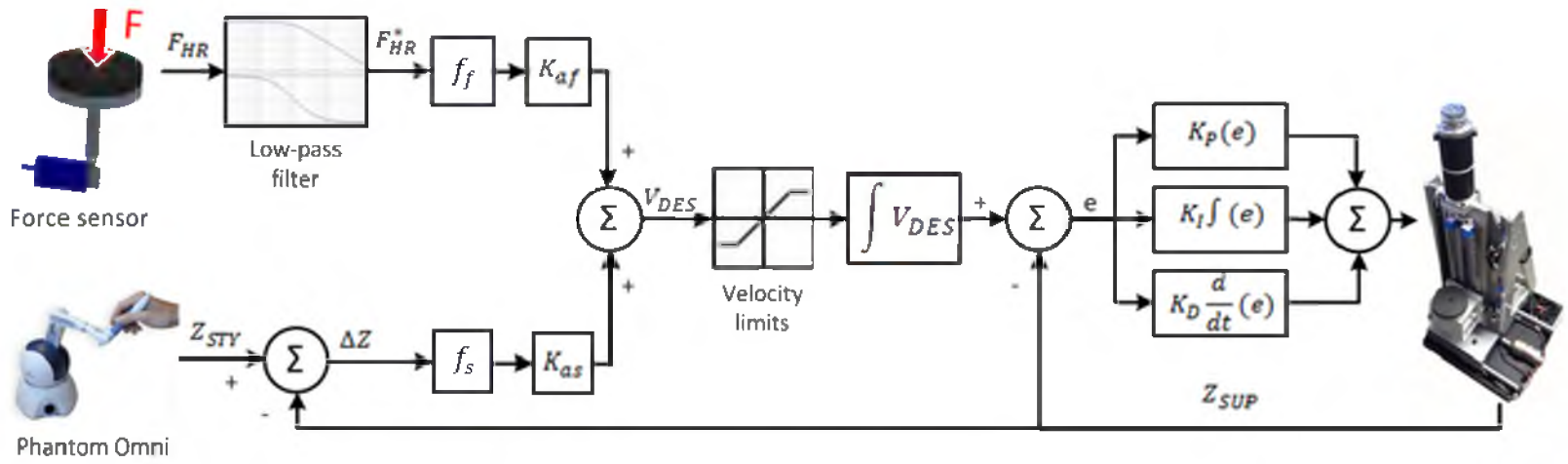

Figure 4.1 Control system diagram for hybrid admittance law. For force input mode assume that f_s is 0, and for stylus input mode assume that f_f is 0. $F_{HR}$is the force relative to the arm weight.

admittance gains for the linear admittance law in the pilot study and for the hybrid controller in the main experiment were set to $125/W_{arm}$ for going up and $150/W_{arm}$ mm/s/N for going down (with W_{arm} measured in N).The result is that the desired velocity will be the same across test participants for a given percentage of the arm weight applied to the support plate. The means of the admittance gains for the pilot study were 9.75 and 11.71 mm/sec/N in the upward and downward directions, respectively.

The squared admittance law is given by:

$$V_{des} = K_a * \left(P_{up} * W_{arm} - F\right)^2 \text{ for } F < P_{up} * W_{arm} \text{ and} \tag{4.2}$$

$$V_{des} = -K_a * (P_{down} * W_{arm} - F)^2 \text{ for } F > P_{down} * W_{arm}. \tag{4.3}$$

P_{up} and P_{down}, like P_{db} in (4.1), are the proportions of W_{arm} that are the limits of the deadband, where P_{up} is slightly less than one and P_{down} is slightly greater than one. A squared admittance law eliminates the discontinuity in acceleration as the force exits the zero velocity dead band region. The admittance gain for this mode was set such that its desired velocity trajectory always intersects that of the linear mode halfway between zero velocity and the velocity limit at 110 mm/s regardless of the weight of the arm. The desired velocity vs. force plot (Figure 4.2) shows how the desired velocity trajectories for the squared and linear admittance control laws compare to each other given W_{arm} = 10 N.

For initial experimentation with both force-based admittance control laws the dead band was set to $0.999* W_{arm}$ to $1.001* W_{arm}$, which for the average weight of a test participant's arm is roughly ±0.013N. This small range was used due to the dynamic nature of the tracking task used in experimentation and based on qualitative assessment. The low-pass filter (8.84 Hz corner frequency) on the force sensor data was implemented in software and reduces the fluctuations of the controller's input forces helping the user to

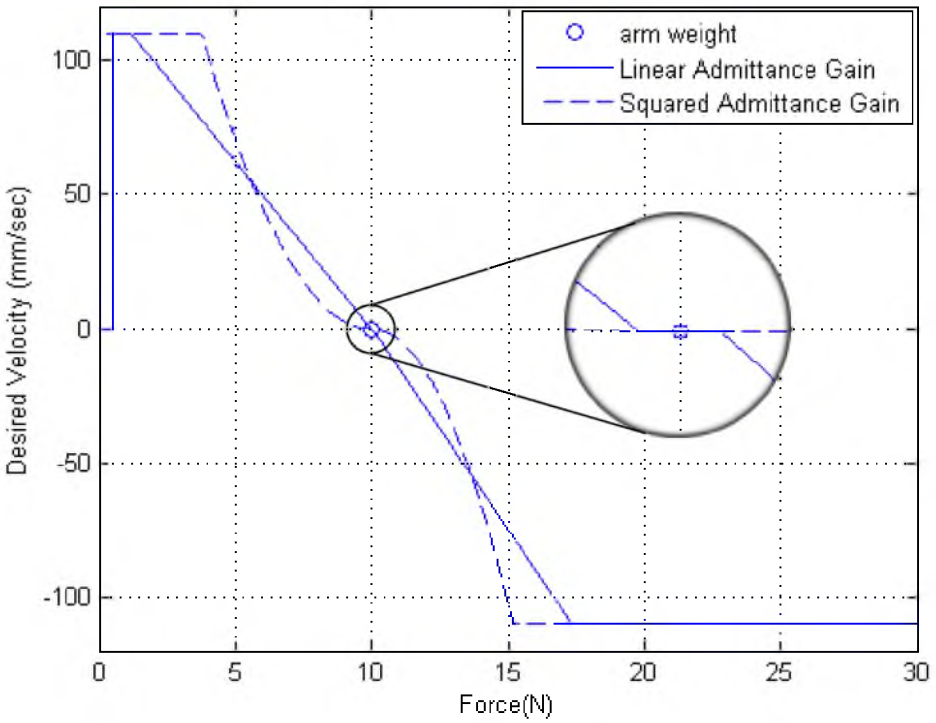

Figure 4.2 The desired velocity of the linear admittance controller compared to the squared admittance controller for a 10 N arm. Note the velocity saturation limit to prevent both controllers from exceeding 110 mm/sec and the drop to zero desired velocity as the force drops below 5% of the arm weight.

maintain a force sensor signal within the dead band when the user intends the VAHR to remain stationary. It was discovered after running the pilot test and first experiment that electrical interference may have been causing the force sensor signal to remain in the dead band after the user's actual force had exited the zero velocity range. It is unsure at this point how this may have affected the initial experimentation, but at least one of the force based admittance modes should be reevaluated in another experiment where electrical noise has been minimized.

4.1.2 Stylus Input

An admittance control law based on the position of the stylus as was investigated by Fehlberg et al. [8] was also examined. This control law takes the form of an admittance

gain multiplied by a virtual spring force (this force is not felt by the user):

$$V_{des} = K_a * K_s(Z_{sty} - Z_{sup}) \quad (4.4)$$

where K_a is a constant admittance gain, K_s is a virtual spring constant and$(Z_{sty} - Z_{sup})$ is the difference between the current position of the stylus and the position of the support plate. Because the zero position of the Omni corresponds to the neutral posture of the user, this distance is representative of the difference between the current position of the wrist and its starting/neutral position. Implementing a dead band of ±2 mm around the zero position of the stylus causes the VAHR to remain stationary unless the stylus deviates from its zero position relative to the stage's position by at least 2 mm. The admittance gains for this controller also differ for upward and downward motion but are not a function of W_{arm}. For the first experiment they were set to 11.24 and 13.49 mm/s/N for upward motion and downward motion, respectively. For the first experiment three different spring constants were evaluated: $K_s = 0.222$, $K_s = 0.445$, and $K_s = 0.667$ N/mm. A comparison of the desired velocity profiles for these three different spring constants is shown in Figure 4.3.

This same governing equation is also used for an elastic control mode, in which a spring force is rendered through the Phantom Omni to the user's hand. This spring force pulls the stylus to its zero position relative to the support plate. Zhai found Elastic rate control to improve precision for an object orientation task under certain conditions [24]. The return spring constant used in the experiment for this controller was 0.18 N/mm and the admittance gains used were the same as those above for the position input mode.

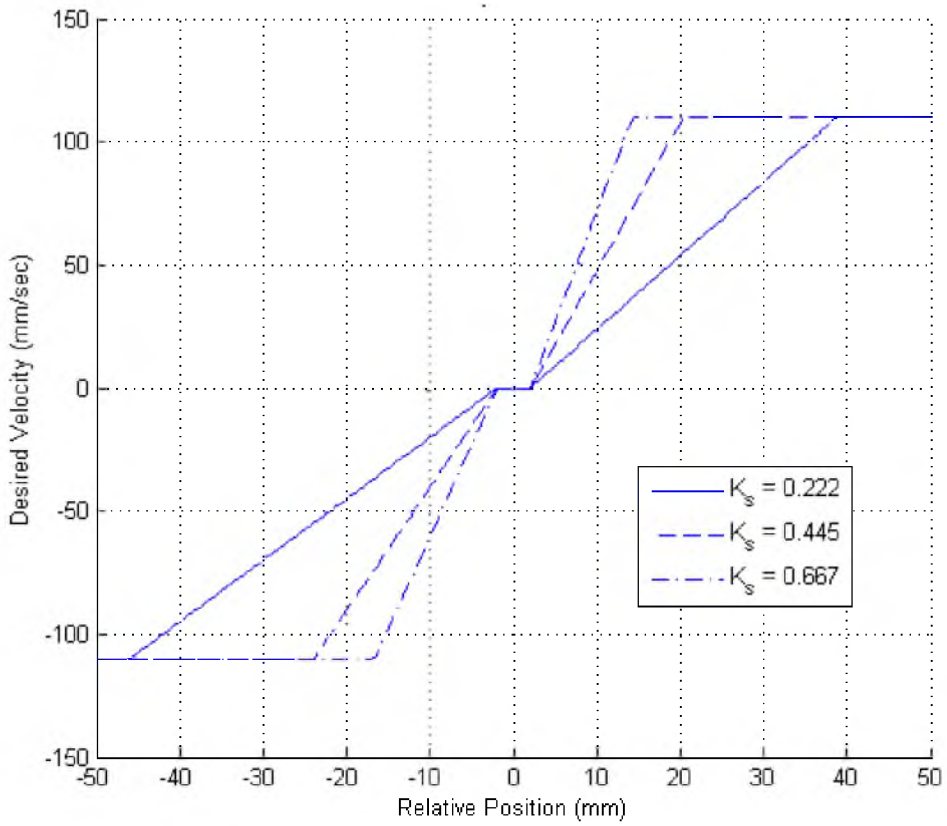

Figure 4.3 The desired velocity of the stylus admittance controller with three different spring constants. Relative position indicates the difference of the stage position from the stylus position. Note the velocity saturation limit to prevent desired velocity from exceeding 110mm/sec.

4.1.3 Hybrid Input Control

A hybrid admittance mode was developed to examine the possibility of improving motion precision by superimposing a force-based admittance law and the position-based admittance law described above. The hybrid admittance control law used can be described by two different equations both of which are helpful for visualization. The first equation is given by

$$V_{des} = f_f * K_{af} * (P_{db} * W_{arm} - F) + f_s * K_{as} * K_s\,(Z_{sty} - Z_{sup}) \tag{4.5}$$

For the first experiment K_{af} was identical to the admittance gains used for the force based linear admittance law and K_{as} was the same as the admittance gain for the position

input controller, namely, $K_{af} = 125/W_{arm}$ and $K_{as} = 11.24$ mm/s/N for upward motion and $K_{af} = 150/W_{arm}$ and $K_{as} = 13.49$ mm/s/N for downward motion. The spring constant used was $K_s = 0.445$ N/mm. Both f_f and f_s take values between 0 and 1 and are set independently of each other. They can be thought of as the fraction of the pure force admittance law (Eqn. (4.1)) (for f_f) and the fraction of the pure stylus admittance law (Eqn. (4.4)) (for f_s) to use in the hybrid admittance law. Implementing the same deadbands described in the previous two sections ensures that forces between $0.999*$ W_{arm} and $1.001* W_{arm}$ and stylus motion within the ±2 mm deadband have no effect on desired velocity. When evaluating the hybrid controller in the main experiment f_f and f_s are set to 0.9 and 0.5, respectively, resulting in an admittance mode where the force on the support plate has the 90% of the effect on desired velocity as in the linear force based controller (Eqn. (4.1)) with the addition of a stylus position based component to desired velocity.

The second equation that can be used to describe the hybrid admittance law, shown below, relates it to the hybrid input mode used by Fehlberg et al. in [8].

$$V_{des} = k_a \left(p * (P_{db} * W_{arm} - F) + (1 - p) * K_s * \left(Z_{sty} - Z_{sup}\right)\right) \tag{4.6}$$

This expression can be thought of as a single admittance gain multiplied by an equivalent force, where the equivalent force is determined as some percentage, p, of the linear force input plus a percentage, $1 - p$, of the virtual spring force computed from the stylus position. Equation (4.6) is equivalent to equation (4.5) for cases where $k_a = f_s * K_{as} + f_f * K_{af}$ and $p = f_f * K_{af}/K_a$.

4.2 PID Controller

The desired velocity obtained from one of the admittance control strategies described above is numerically integrated to obtain a target position, and a PID controller is implemented to drive the actual position of the stage to the target position, the equation of which is shown below.

$$DAC\ Voltage = K_p * Error + K_i * (\Sigma Error * t) - K_d * (Z_{current} - Z_{previous})/t \quad (4.7)$$

K_p, K_i, and K_d are the proportional, integral and derivative gains, $Error$ is the current difference between the desired and the actual position and $Z_{current}$ and $Z_{previous}$ are the positions of the stage at the current and previous time steps. The PID gains were adjusted to maximize responsiveness and to minimize stick-slip behavior of the stage. Responsiveness and stick-slip behavior were evaluated qualitatively based on haptic interaction with the device. The PID gains are set to be as follows: K_p = 5 V/mm, K_i = 10 (V/sec)/mm, K_d = 0.12 V/(mm/sec). In software the voltage set by the PID controller is limited to ±10V and the contribution of the integral term is limited to |5V|. Figure 4.4 shows the typical performance of the PID controller at driving the actual position of the VAHR to a desired position that is set to be a sine wave. The sine wave shown has a frequency of 0.2 Hz and a peak-to-peak distance of 85 mm. This combination of frequency and amplitude produces a sine wave in which the maximum vertical velocity is approximately equal to the 110 mm/sec velocity limit, thus this sine wave is reflective of the fastest speed that would ever be encountered during the tracking experiment. The actual position lags behind the desired position slightly, and the error between the desired and actual positions is limited to roughly 7 mm, which can be easily compensated for by the user's wrist motions.

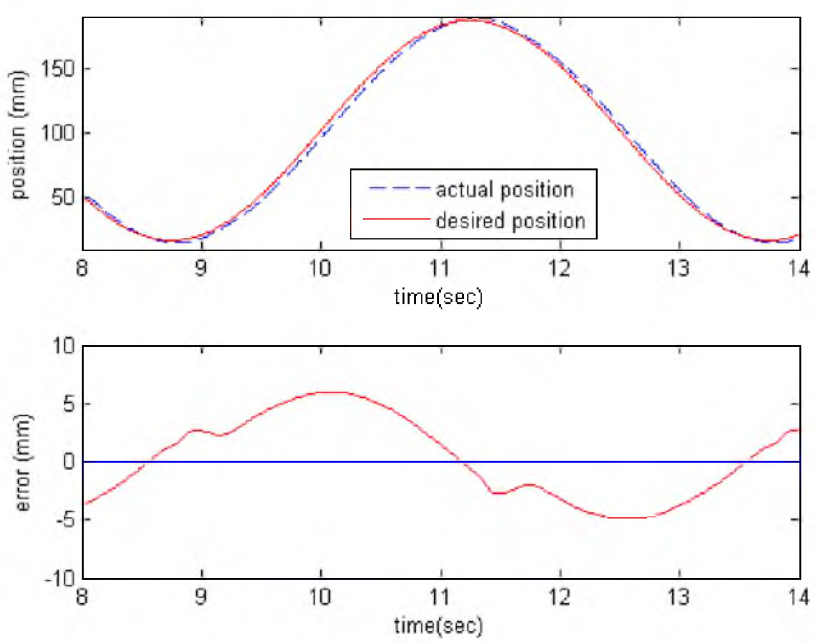

Figure 4.4 PID controller performance given a sine wave input for desired position. The top graph shows the desired and actual positions, and the bottom graph shows the error between the actual and desired positions.

Figure 4.5 shows the frequency response of the PID controlled VAHR given sinusoidal inputs of ±5 mm, ±25 mm, and ±45 mm amplitudes. The large motion (±45 mm amplitude) bandwidth for the VAHR is roughly 2 Hz, and the small motion (±5 mm amplitude) bandwidth is 4 Hz. Although the tracking performance of the VAHR would be unacceptable in many systems that require precise position control it is acceptable in this case for several reasons. First, the PID gains were not tuned to achieve perfect position tracking, but to yield smooth, steady interaction with the user. The fact that the actual position lags the desired position slightly helps avoid jerky motions. Second, in practice the desired velocity is not set based on a predefined trajectory, but on the force or stylus position input of the user.

During experimentation a participant supplies a control input based on the path they are attempting to track, and based on how they believe the VAHR will respond. In this

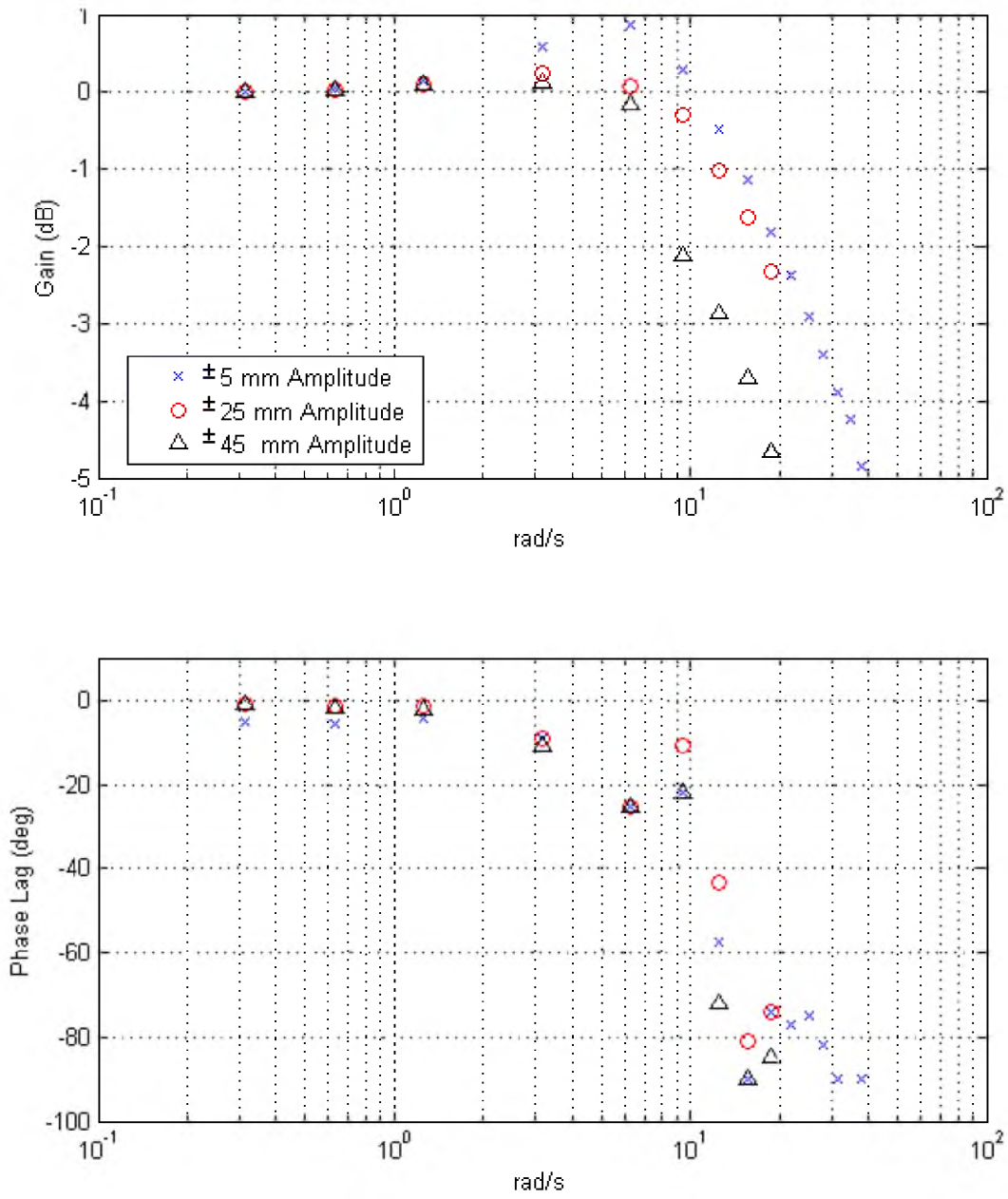

Figure 4.5 Frequency response of the closed loop system (VAHR with PID controller) showing the tracking performance for sinusoidal inputs of three amplitudes. The motion bandwidth is approximately 2 Hz (12.6 rad/sec) for ±45 mm amplitude sinusoids and 4 Hz (25.1 rad/sec) for ±5 mm amplitude sinusoids.

sense, the "desired position" that is passed to the PID controller is somewhat arbitrary as it is not equal to the position that the participant actually desires. Furthermore, each participant adjusts his/her control input according to the response of the VAHR, and in this way each participant acts as his/her own closed loop controller. The most important concern in implementing a controller on the VAHR is not that it perfectly tracks a virtual position trajectory, but that its response to user input is intuitive.

CHAPTER 5

EXPERIMENT DESIGN AND RESULTS

To evaluate the vertical active handrest, an experiment paradigm that tested the ability of participants to accurately complete a precision dexterous task with and without the assistance of the VAHR was necessary. To have a statistically meaningful outcome, the experiment needed to be difficult enough that participants would not perform perfectly (either with or without the use of the VAHR) to avoid a ceiling effect. It was also desired that the experiment paradigm require only one DOF motion in the vertical axis in order to evaluate the effects of using the VAHR without adding confounding factors from requiring motion in other axes. Three experiment paradigms were considered: A targeting task similar to the one presented by Fitts in [25], a membrane piercing task (e.g., [26]), and a tracking task in which participants would track a horizontally scrolling path (essentially a "pursuit" tracking task as described by Jagacinski and Flach [27]).

In a Fitts type targeting task designed for the VAHR two target regions, which could be implemented either physically or virtually, would be oriented on a vertical plane and separated by some distance within the workspace of the device along a vertical axis. Each trial would consist of the participant tapping (or perhaps clicking on) each target region as many times as possible in a limited amount of time, alternating between the two targets. Timing and accuracy data would be collected and analyzed for each trial. Given

the velocity limitations of the VAHR it would likely be uninteresting to compare various VAHR controller conditions to the freehand case for this targeting task, although it might be useful to make comparisons between different VAHR conditions.

In a membrane piercing task participants would use a needle to pierce a thin semiflexible membrane while attempting to minimize the force applied to a soft substrate slightly below the membrane once piercing was accomplished, similar to the piercing task presented by Kontarinis et al. for evaluating the effects of force and vibration feedback in teleoperation tasks [26]. A membrane piercing task could be implemented using either a real membrane and needle or via a haptic simulation. Participants would attempt the task with various support conditions, including freehand, fixed wrist support, and VAHR support. While the results of a membrane piercing task might show that forces applied to the substrate could be reduced by using the VAHR it would not utilize much of the device's workspace.

In order to best exploit the workspace of the VAHR a tracking task was chosen as the initial experiment paradigm. In a tracking task it is possible to structure the target path(s) such that both rapid and slow, steady motions and movements of both small and large magnitudes are required.

5.1 Tracking Task Design

A single-axis vertical tracking task was designed to investigate the effectiveness of the VAHR in aiding with a precision dexterous task. In experiments, participants are asked to maintain the position of a small spherical cursor between the upper and lower borders of a sinusoidal path. The upper and lower bounds are 10 mm apart. This separation distance was found to yield a moderately difficult tracking task in conjunction

with the other path parameters based on qualitative evaluation during preliminary testing. The position of the Omni's stylus directly controls the position of the sphere. The paths scroll from right to left at a constant horizontal velocity of 50 mm/sec each path lasting for two minutes. The motion of the paths and the vertical motion of the stylus are displayed at approximately 2.5:1 scale on the screen such that the velocity of any given point on a path moves across the screen at 12.7 cm/s. This is with the experiment window maximized to full screen on a 51 cm wide monitor. While the velocity at which the path translates across the screen would change with a different sized monitor (or with a smaller viewing window on the existing monitor) the physical velocity of the path (50 mm/sec) will not change. Both the motion of the sphere on the screen and the motion of the stylus are constrained to move along a vertical line. The location of the stylus is displayed as a green sphere so long as it is between the upper and lower bounds of the path. When the stylus position leaves the borders of the given path, the color of the ball changes to red and will remain red until the stylus position returns to within the bounds of the path. Two types of paths were generated; paths with lower frequency tracking features and paths with higher frequency tracking features. Screenshots of the tracking task in Figure 5.1 show examples of both high and low frequency paths. Both types are composed of 20 random sine waves superimposed. The superposition of sine waves of various amplitudes, frequencies and phases is presented by Jagacinski and Flach as a simple and effective way of creating a path for a tracking task [27]. Morris et al. used a similar method in [28] for constructing force trajectories.

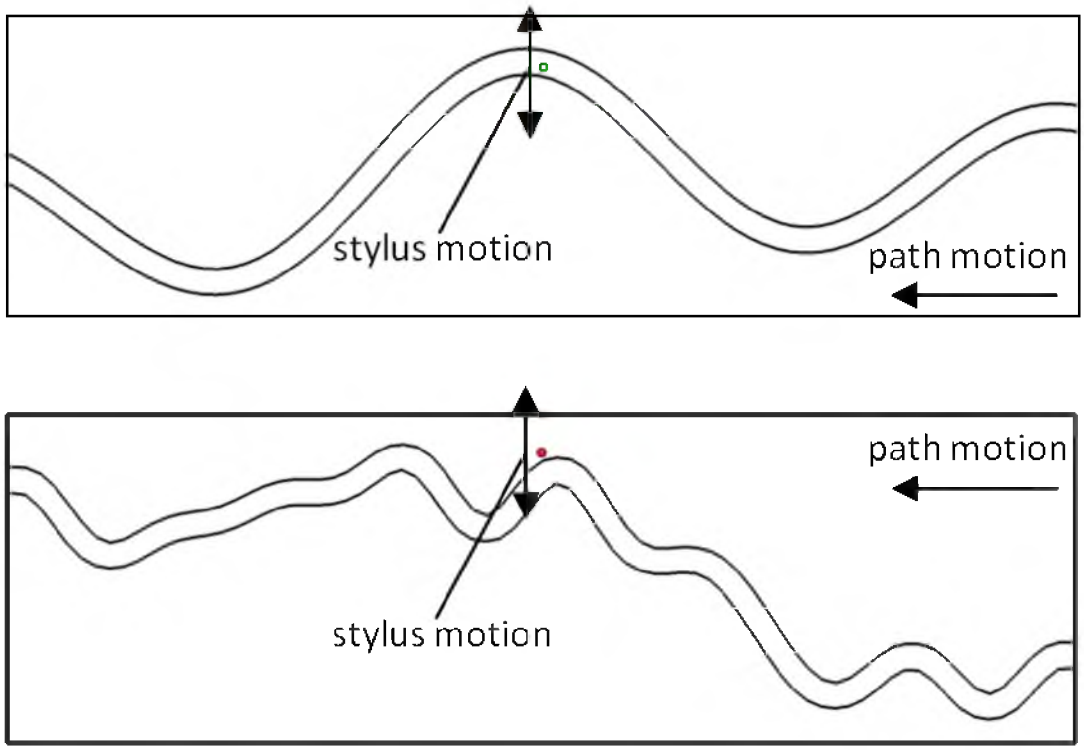

Figure 5.1 A portion of the low-frequency path (top) and a portion of high-frequency path (bottom). The sphere shows the current stylus position

5.2 Path Generation

The sequence used in generating the low and high frequency paths is described here in a series of steps.

Step 1

Twenty sine waves of the form (5.1) with random amplitudes, A, and frequencies, F, are generated, where t increases in increments of 0.01 sec and z is in mm.

$$z = A\sin(F * t) \tag{5.1}$$

For low-frequency paths the 20 sine waves are assigned frequencies between 0 and 0.64 Hz (note that these values must be scaled by 2π as F is in radians/sec rather than Hz) and amplitudes between 0 and 15 mm. For high-frequency paths 15 of the sine waves have

the same characteristics as those used for low-frequency paths and 5 sine waves are assigned frequencies between 1 and 3 Hz and amplitudes between 0 and 5 mm. These frequencies and amplitudes give the desired results for the general shape of a path, but are not reflective of the amplitudes and frequencies of the final paths, as both the magnitude and frequency are scaled as is described in later steps. The ranges of amplitudes and frequencies stated above for the low- and high-frequency paths were chosen based on qualitative assessment of the difficulty of tracking the resulting paths after the steps to alter magnitude and frequency were applied (described below). These ranges were chosen to yield a tracking task that would not be so frustrating that test participants would give up, but would be difficult enough to cause tracking errors in a vast majority of trials. These initial ranges of amplitude and frequency were later verified by the performance of test participants: in only three trials out of 196 for the main experiment did participants achieve perfect tracking accuracy, and only one participant exhibited frustration to the point of partially giving up on one trial.

Step 2

The sine waves generated in step one are summed to obtain an initial path, P, which is given by:

$$P = A_1 \sin(F_1 * t) + A_2 \sin(F_2 * t) + \cdots + A_{20} \sin(F_{20} * t) \tag{5.2}$$

Step 3

The maximum and minimum of path P, representing the highest ($\max(P)$) and lowest ($\min(P)$) points on the path respectively are found. The range spanned by the path is given by $\max(P) - \min(P)$.

Step 4

The amplitude of the path is scaled by a scaling factor, G, in order to achieve the desired range, R_{des}, where G is given by:

$$G = \frac{R_{des}}{\max(P) - \min(P)} \tag{5.3}$$

For experimentation with the VAHR the desired path range is set to 175 mm. This results in a modified path given by:

$$P' = G * A_1 \sin(F_1 * t) + G * A_2 \sin(F_2 * t) + \cdots + G * A_{20} \sin(F_{20} * t) \tag{5.4}$$

Step 5

The derivative of the modified path ($\frac{dP'}{dt}$) is taken, and the maximum of the absolute value, $\left|\frac{dP'}{dt}\right|$, is found in order to determine the maximum slope of P' in mm/sec, which correlates to the maximum vertical velocity required of the VAHR in order to track the path. The derivative of P' is given by

$$\frac{dP'}{dt} = G * A_1 * F_1 \cos(F_1 * t) + G * A_2 * F_2 \cos(F_2 * t) + \cdots + G * A_{20} * F_{20} \cos(F_{20} * t) \tag{5.5}$$

and the maximum slope is

$$\text{max slope} = \max\left(\left|\frac{dP'}{dt}\right|\right) \tag{5.6}$$

Step 6

The maximum slope obtained in (5.6) can be altered by multiplying (5.5) by a scalar. For experimentation with the VAHR it is desired that (5.5) be scaled by J in order that the maximum slope of the path is equal to the velocity limit, V_{lim}, of the VAHR, where J is given by:

$$J = \frac{V_{lim}}{\max\left(\left|\frac{dP'}{dt}\right|\right)} \tag{5.7}$$

The derivative of P' cannot, however, be scaled without modifying the path of equation (5.4), thus a method for altering the maximum slope of P' without affecting the range set in step 4 is required. This is achieved by multiplying the frequencies of the original 20 sine waves by J. This results in the following equations for the final path and its derivative.

$$P_f = G * A_1 \sin(J * F_1 * t) + G * A_2 \sin(J * F_2 * t) + \cdots + G * A_{20} \sin(J * F_{20} * t) \tag{5.8}$$

$$\frac{dP_f}{dt} = G * A_1 * J * F_1 \cos(J * F_1 * t) + G * A_2 * J * F_2 \cos(J * F_2 * t) + \cdots + G * A_{20} * J * F_{20} \cos(J * F_{20} * t) \tag{5.9}$$

Step 7

After the initial amplitude and frequency have both been scaled to obtain the path in (5.8) the second and third derivatives of P_f are taken, which represent the acceleration and jerk of the path respectively. In order to further promote uniformity between randomly generated paths, limits are placed on the acceleration and jerk, but because there are no other parameters to be modified that would not change the constraints already placed on the path this must be done by trial and error. The averages of the absolute values of acceleration and jerk are compared to their respective limits, and if they do not fall within their acceptable ranges the path generation process is started over. For low-frequency paths the averages of the absolute values of acceleration and jerk are limited to be within the ranges of 11-13 mm/sec^2 and 6-8 mm/sec^3 respectively. For high frequency paths the acceptable ranges are set to 60-70 mm/sec^2 for acceleration and 180-

190 mm/sec^3 for jerk. Similar to the method for assigning the initial path amplitudes and frequencies of step one these ranges for acceleration and jerk were assigned based on qualitative assessment of tracking difficulty. For low-frequency paths the allowable ranges for acceleration and jerk were narrowed until the resulting tracking difficulty was uniform between randomly generated low-frequency paths. This same procedure applies to the acceptable ranges for high-frequency paths.

Step 8

After an acceptable path is obtained by following steps one through seven, two offset curves must be defined, one above and one below the generated path, to serve as upper and lower bounds for the tracking task. During the tracking task the test participant attempts to keep the cursor between these two bounds, while the final path of (5.8) is not displayed to the user at all. For each of the two offset curves one point is produced for every point of the final path, which has 1 point every 0.01 sec. In other words, at any time t_i that is a multiple of 0.01 sec there is one point for each of the offset curves and for the path given by (5.8). The steps taken to produce the two offset curves are described below, where t_i is the time at the time step of interest and t_{i+1} is the time at the next time step, i.e., $t_{i+1} = t_i + 0.01$ sec.

1. Obtain a vector parallel to the path at t_i:

$$\overrightarrow{v_1} = \left(0, t_{i+1} - t_i, P_f(t_{i+1}) - P_f(t_i)\right) \tag{5.10}$$

2. Find a vector perpendicular to $\overrightarrow{v_1}$ by taking the cross product of $\overrightarrow{v_1}$ with (1,0,0) and scale this vector to be the same magnitude as the offset distance:

$$\overrightarrow{v_2} = offset * \frac{\overrightarrow{v_1} \times (1,0,0)}{|\overrightarrow{v_1} \times (1,0,0)|} = (0, t_2, p_2) \tag{5.11}$$

3. Compute the equation of a line that is parallel to the path at t_i and is offset by the desired offset distance:

$$P_{\parallel} = \frac{dP_f}{dt}(t_i) * t + intercept \tag{5.12}$$

where $\frac{dP_f}{dt}(t_i)$ is the slope of the path at t_i and the intercept can be solved for as:

$$intercept = p_2 + P_f(t_i) - \frac{dP_f}{dt}(t_i) * (t_2 - t_i) \tag{5.13}$$

4. Calculate the point of the boundary curve at t_i:

$$B(t_i) = P_{\parallel}(t_i) \tag{5.14}$$

As recorded here these steps produce the lower offset curve given a right handed coordinate system, they are repeated with minor sign changes to produce the upper offset curve. A graphical representation of these steps is shown in Figure 5.2. The upper and lower boundaries in the figure are shown at a one mm offset for graphical purposes, for experiments these curves are offset from the final path curve by five mm.

5.3 Test Procedures

For both the pilot study and first experiment, participants rested their right arm on the support plate of the VAHR while grasping the stylus of the omni at the beginning of each study so that both the force sensor and the stylus position could be tared to the weight and neutral posture of his/her arm. Participants were instructed to move the stylus up and down to maintain the cursor position between the two path boundaries as the path scrolled from right to left across the screen. Before starting actual experiments each participant was allowed to practice with a subset of the controllers to be tested until they were sufficiently comfortable with using the VAHR and with the vertical tracking task. Tracking data was then gathered for the various VAHR control modes being tested as

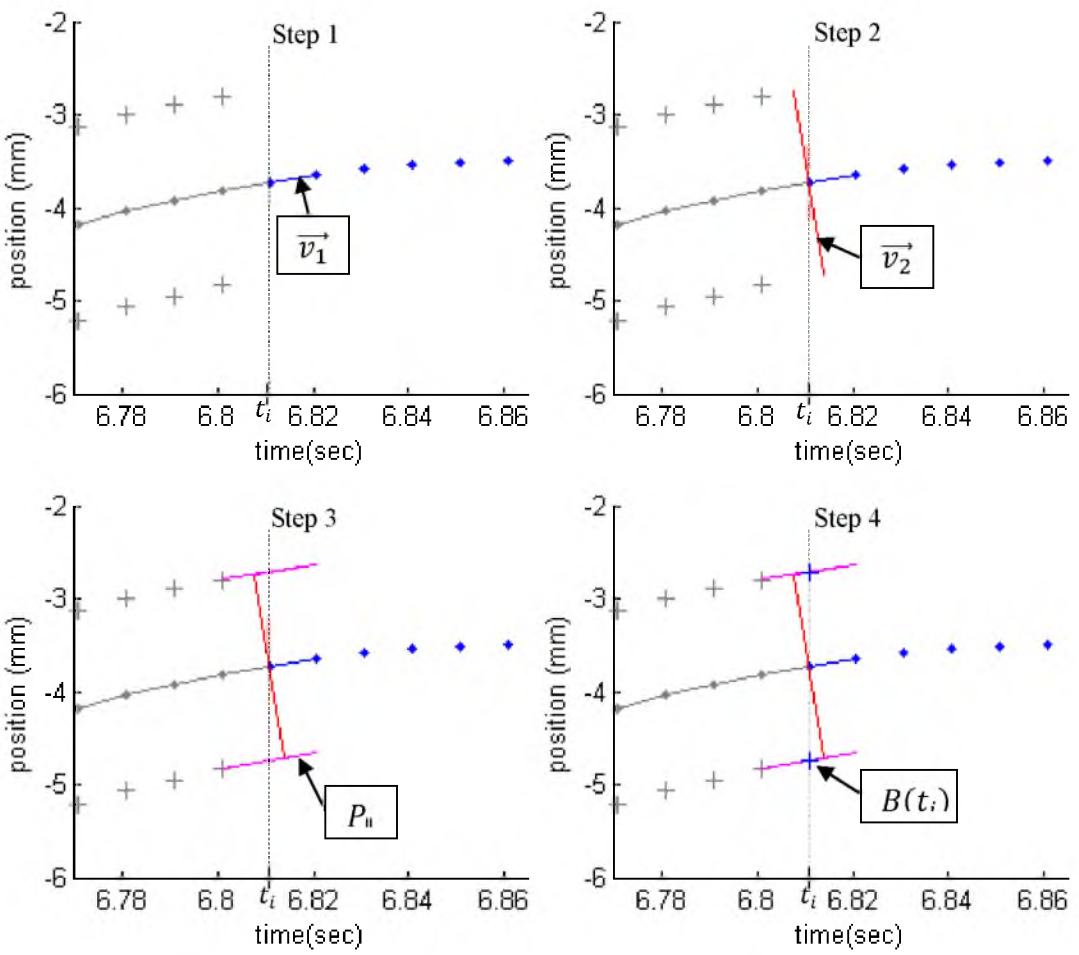

Figure 5.2 Steps for offsetting the curve to generate upper and lower boundaries. The boundaries in the figure are offset by one mm for graphical purposes, for experiments the boundaries are offset from the path curve by five mm.

well as for several conditions in which the VAHR was not used. The non-VAHR support conditions tested for the pilot study and the first experiment included a fixed elbow rest, a fixed wrist rest, and no support (i.e., freehand). For each support condition test participants completed one low-frequency path followed by one high-frequency path.

Participants wore headphones playing pink noise to reduce distractions and to mask ambient noise. All participants used their right hand regardless of their dominant hand. In order to minimize the effects of test order, such as fatigue and learning, a Latin squares

approach was used to generate orders in which participants would experience each support condition. To further reduce the effects of fatigue, participants were encouraged to take a break between support conditions until they felt rested.

At the end of each study, participants rated on a scale from 1 to 5, how easy they felt it was to stay inside each path (both low- and high-frequency) with each support condition and how fatigued they felt after using each support condition. The position of the stylus and the path data for each trial were recorded for later analysis. Data were not recorded during the first 5 seconds of each trial, giving the user time to adjust to the new support condition.

5.4 Participant Performance Evaluation Criteria

Jagacinski and Flach suggest several evaluation metrics for tracking performance including percent time on target, mean absolute error and root mean squared (RMS) error, where RMS error is the most common measure for tracking performance [27]. Each of these metrics was examined in the evaluation of the experimental data. One other metric was also examined, namely the number of errors, or the number of excursions from the path. A similar metric was used by Bardorfer et al. for evaluating accuracy in labyrinth navigation, the difference being that they examined the number of collisions rather than excursions, as the cursor could not pass through the walls of the labyrinth [29]. In the context of the VAHR the number of excursions could represent the number of times an artery is hit during surgery, or the number of times a delicate component is nicked in an assembly task. For each of the performance metrics listed here an accuracy rating is assigned to each trial, i.e., there is one accuracy rating per participant for each path frequency and support condition combination.

For percent time on target this accuracy rating is the time during each trial that the cursor was within the path boundaries divided by the total trial time. For the mean absolute error and the RMS error the path accuracy rating is obtained by summing either the absolute value of the error or the squared error, respectively, for each point and then taking the mean of this value. The square root of this mean is then taken for RMS error. As suggested by Jagacinski and Flach for paths of finite width, error is defined as the distance from the cursor to the nearest path boundary, and is set to zero for points within the path boundaries (Figure 5.3) [27]. The path accuracy rating for number of excursions is simply the number of times the cursor crosses out of the path boundaries, an example path section from a high-frequency trial showing six excursions is shown in Figure 5.4.

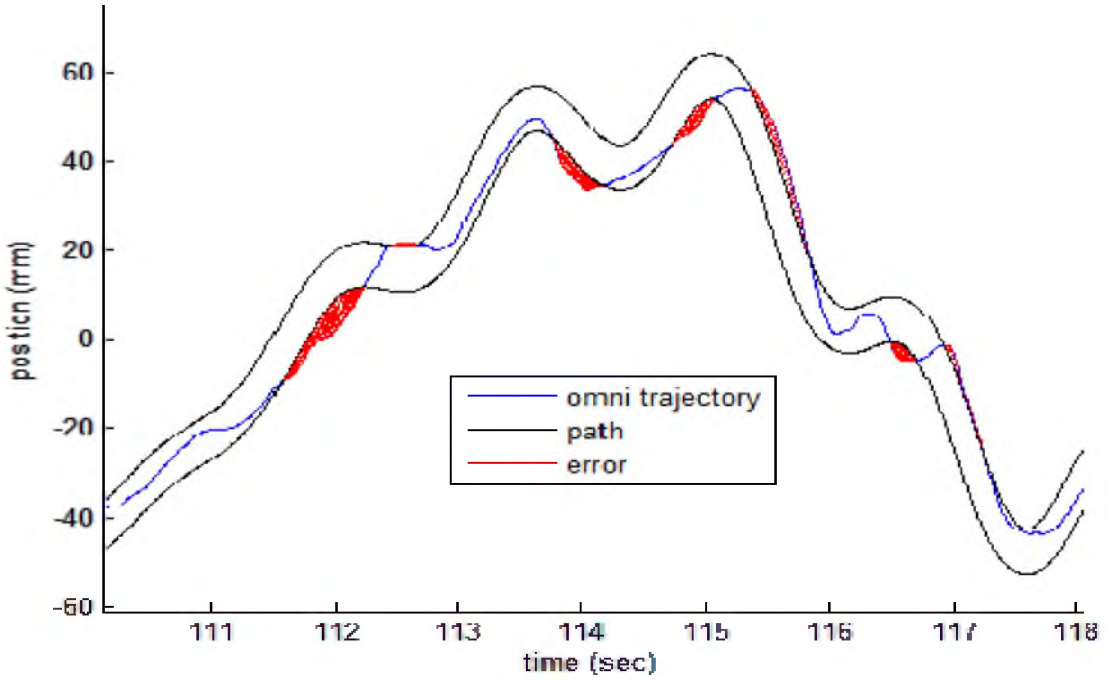

Figure 5.3 Example path section including stylus trajectory. The error is represented by the filled in regions between the stylus trajectory and the path boundaries.

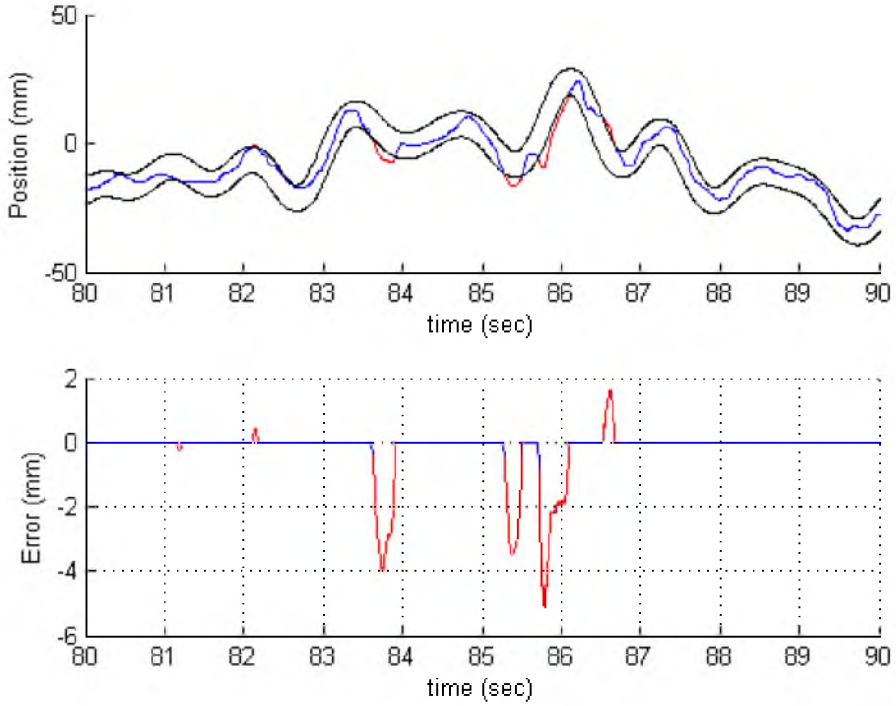

Figure 5.4 A 10 second sample of a high-frequency path with the trajectory of the cursor (top) and the corresponding error (bottom). In this example there are six excursions. (The trajectory of the stylus is shown in blue while it is inside the borders and in red when outside.)

The null hypothesis that all the support conditions tested perform equally for the tracking task is tested by passing the path accuracy ratings into a two way repeated-measures Analysis of Variance (ANOVA), where the two factors are support condition and path frequency (either high or low). A repeated measures analysis is used because each participant is evaluated under all experimental conditions. Using a repeated-measures ANOVA helps compensate for the variance introduced as a result of each participant's individual level of fine motor control by removing between subjects variance [30]. Mauchly's test is used on each set of accuracy ratings to determine whether the assumption of sphericity, which is made in repeated-measures ANOVA, is valid. If Mauchly's test yields a significant result, i.e., if the assumption of sphericity is

not met, then Greenhouse-Geisser correction is applied to reduce the degrees of freedom before the repeated-measures ANOVA is performed [31]. For ANOVA results that reject the null hypothesis that all support conditions yield the same level of tracking performance Fisher's Least Significant Difference (LSD) test is used to determine which support conditions yield a statistically different level of tracking performance from the others. An alpha level of 0.05 is used to distinguish between significant and nonsignificant results.

5.5 Pilot Study Results – Force Input

The pilot study was conducted to validate the functionality of the VAHR and to gain insight through experimental interactions with naive participants by gathering user performance and opinion data. The study examined five support conditions for use with the path tracking task. There were five participants (two female), ages 19 to 31, three of whom were right hand dominant by self-report. The support conditions tested included free hand, fixed wrist support, fixed elbow support, VAHR with the force based linear admittance controller (Eqn. (4.1)), and VAHR with the force based squared admittance controller (Eqns. (4.2) and (4.3)). Participants used each support condition to track one low frequency path and one high frequency path, where the low frequency path always preceded the high frequency path. Each path was randomly generated according to the procedure described in Section 5.2. Using a number of participants that is a multiple of the number of support conditions is important for Latin squares ordering to effectively limit the effects of test order such as learning and fatigue. Figure 5.5 shows the configuration of the arm and the support plate for each support condition. In practice the support plate of the VAHR is used for both the fixed wrist and fixed elbow support

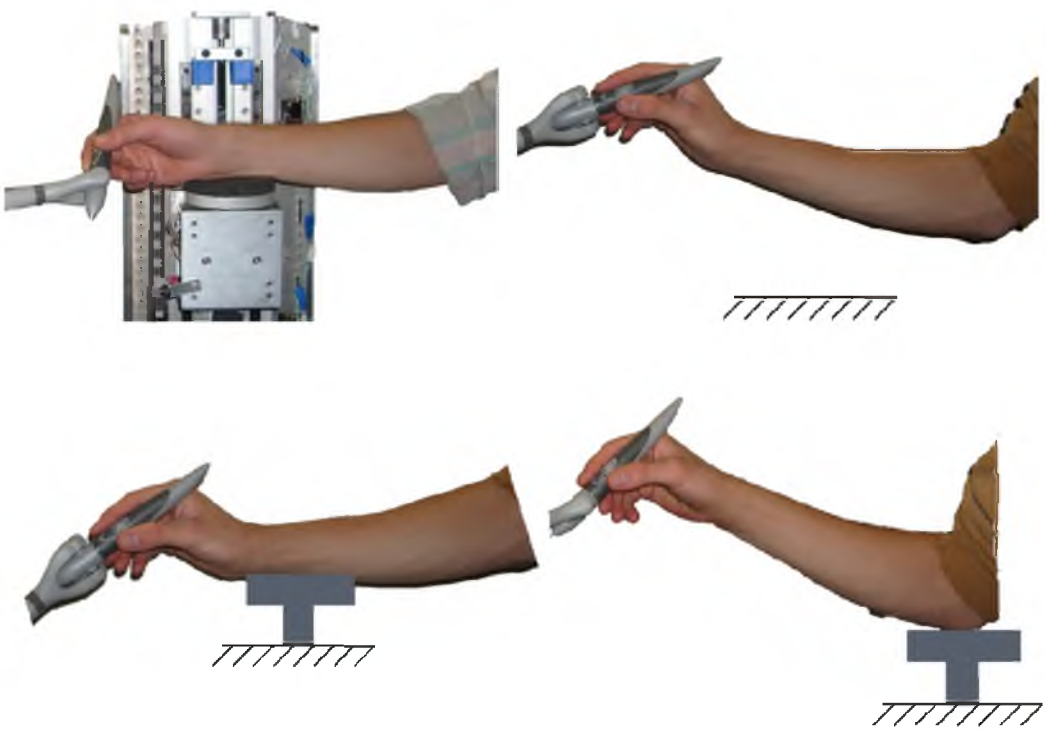

Figure 5.5 Support Condition postures, VAHR modes (top left), Freehand (top right), fixed wrist rest (bottom left), and fixed elbow rest (bottom right).

conditions with the position of the stage remaining fixed. In addition to tracking performance data, participant opinion data was gathered using a questionnaire. Each participant ranked the ease of maintaining the cursor within the boundaries of the path and also their perceived level of fatigue under each support condition and for each path frequency. Two example sections from the questionnaire are shown in Figure 5.6. For the main experiment participants filled out a similar questionnaire but did not rank the support conditions separately for high- and low-frequency paths in terms of the perceived fatigue, rather each support condition was ranked independently of path frequency.

Box plots (Figure 5.7) show the accuracy ratings for all evaluation metrics for each support condition for both high- and low-frequency paths. The median of each group is represented by a red line and the bottom and top edges of each box represent the 25th and

On a scale from 1 to 5 rate the difficulty of tracking the LOW FREQUENCY sine wave path using each of the following support conditions, where 1 = Very Easy, 2 = Easy, 3 = Moderate, 4 = Difficult, and 5 = Very Difficult		
VAHR, Controller L		
VAHR, Controller S		
Freehand		
Fixed Wrist Rest		
Fixed Elbow Rest		

On a scale from 1 to 5 rate how fatigued your arm felt after tracking the LOW FREQUENCY sine wave path using each of the following support conditions, where 1 = Not At All Fatigued, 2 = Slightly Fatigued, 3 = Moderately Fatigued, 4 = Fatigued, and 5 = Very Fatigued		
VAHR, Controller L		
VAHR, Controller S		
Freehand		
Fixed Wrist Rest		
Fixed Elbow Rest		

Figure 5.6 Example questionnaire sections for tracking difficulty (top) and arm fatigue (bottom) for low frequency paths.

75th percentiles, respectively. The whiskers extend out to the furthest points of each group that are within 1.5 times the interquartile range from the box boundaries, where the interquartile range is the range between the 25th and 75th percentiles. Outliers are identified as points beyond the whisker length and are denoted on the box plots by plus signs. The box plots show that tracking performance varied widely between participants for some of the support conditions, and not for others (indicated by the size of the interquartile region). The data for the freehand case is more tightly clustered than for the VAHR support conditions, perhaps indicating that some participants had more trouble interacting with the device than others. It is also clear from the four box plots that data for many of the groups are not normally distributed (the median is not in the center of the box). ANOVA analysis assumes a normal distribution but is used on these data anyway as it has been shown to be robust against violations of this assumption [32].

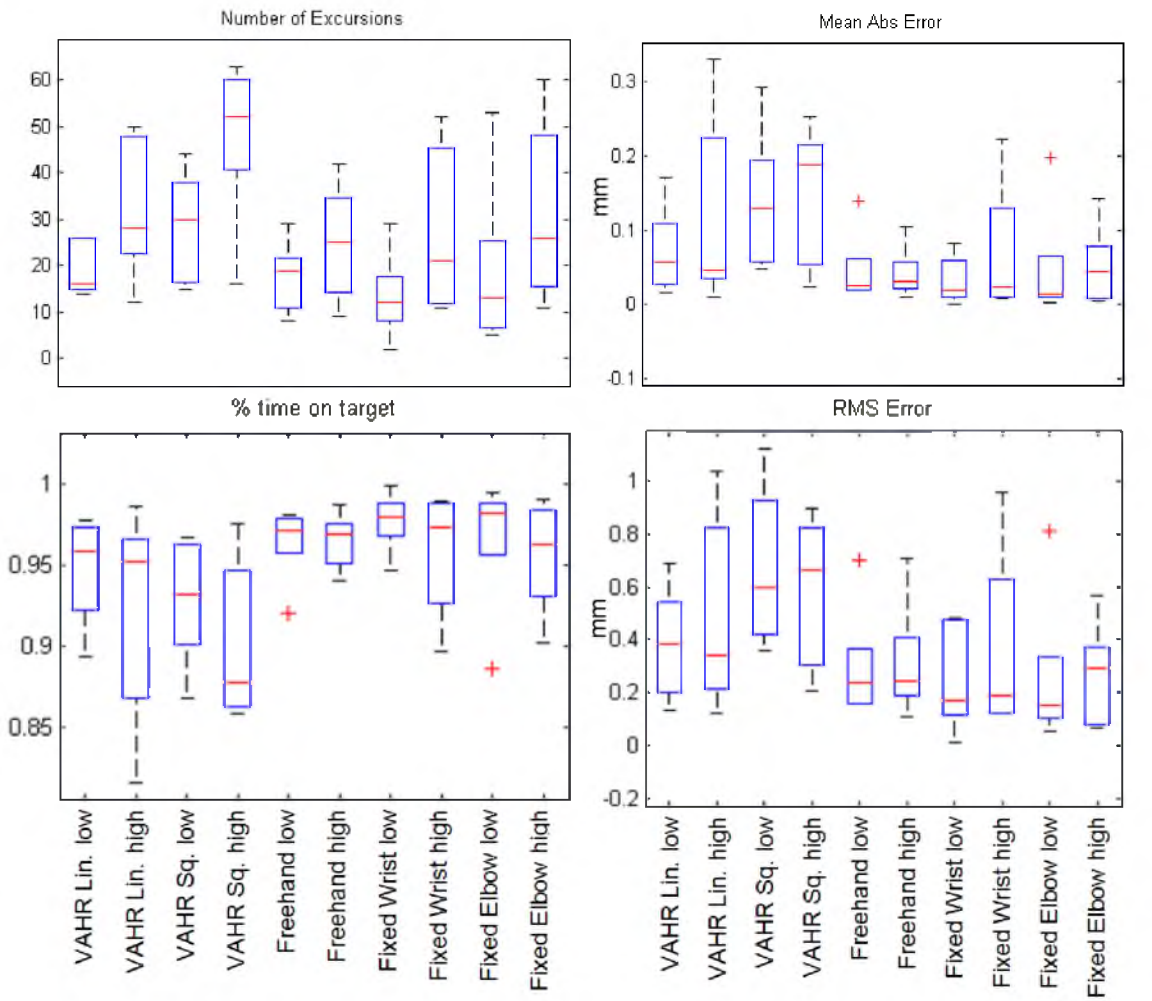

Figure 5.7 Box plots for number of excursions(top left), mean absolute error (top right), percent time on target (bottom left) and RMS error (bottom right) showing high and low frequency tracking performance for each support condition in the pilot study. For percent time on target 1 correlates to 100 %.

The repeated-measures ANOVA described in Section 5.4 rejects the null hypotheses for all four evaluation metrics that all the support conditions tested yield the same accuracy rating; [$F(4,16) = 5.08$, $p = 0.0078$] for percent time on target, [$F(4,16) = 4.95$, $p = 0.0087$] for RMS error, [$F(1.96,7.84) = 5.04$, $p = 0.04$] for number of excursions and [$F(4,16) = 3.64$, $p = 0.0271$] for mean absolute error. Note that the data for number of excursions did not meet Mauchly's sphericity criterion (chi-square(9) = 19.49, $p = 0.049$) so the degrees of freedom were adjusted using the Greenhouse-Geisser estimate of

sphericity ($\varepsilon = 0.49$). The mean and 95% confidence interval of participants' accuracy ratings for each of the four evaluation metrics is shown are Figure 5.8. The data in this figure have been adjusted to remove the between subjects variance, better reflecting the repeated measures analysis, according to the procedure presented by Cousineau [30]. Visual comparison of the groups in Figure 5.8 gives an idea of which comparisons might be found to be significant according to Fisher's LSD. The results of Fisher's LSD test show which support conditions had significantly different performance than the others at the $\alpha = 0.05$ level. The only significant differences shown in tracking performance between the various support conditions for any of the evaluation metrics are between the VAHR with the squared admittance controller and the non-VAHR support conditions. According to the percent time on target, RMSE, and mean absolute error metrics the squared admittance controller support condition performed significantly worse than both of the fixed supports and freehand ($p \leq 0.044$). For the number of excursions metric the squared admittance support condition was outperformed by freehand and fixed wrist conditions ($p \leq 0.013$). The VAHR with the linear force controller is also outperformed by the non-VAHR conditions, although not significantly so.

The results of the questionnaire described above were analyzed using a one-way ANOVA followed by Tukey's HSD to determine which support conditions yielded significantly different responses. For low-frequency paths, most participants perceived the VAHR linear admittance controller, freehand and fixed elbow rest to be easier to maneuver through the path compared to the VAHR squared admittance controller and fixed wrist rest, but no statistical significance was found (Figure 5.9 left). For the high-frequency case, participant responses showed that they perceived freehand and fixed

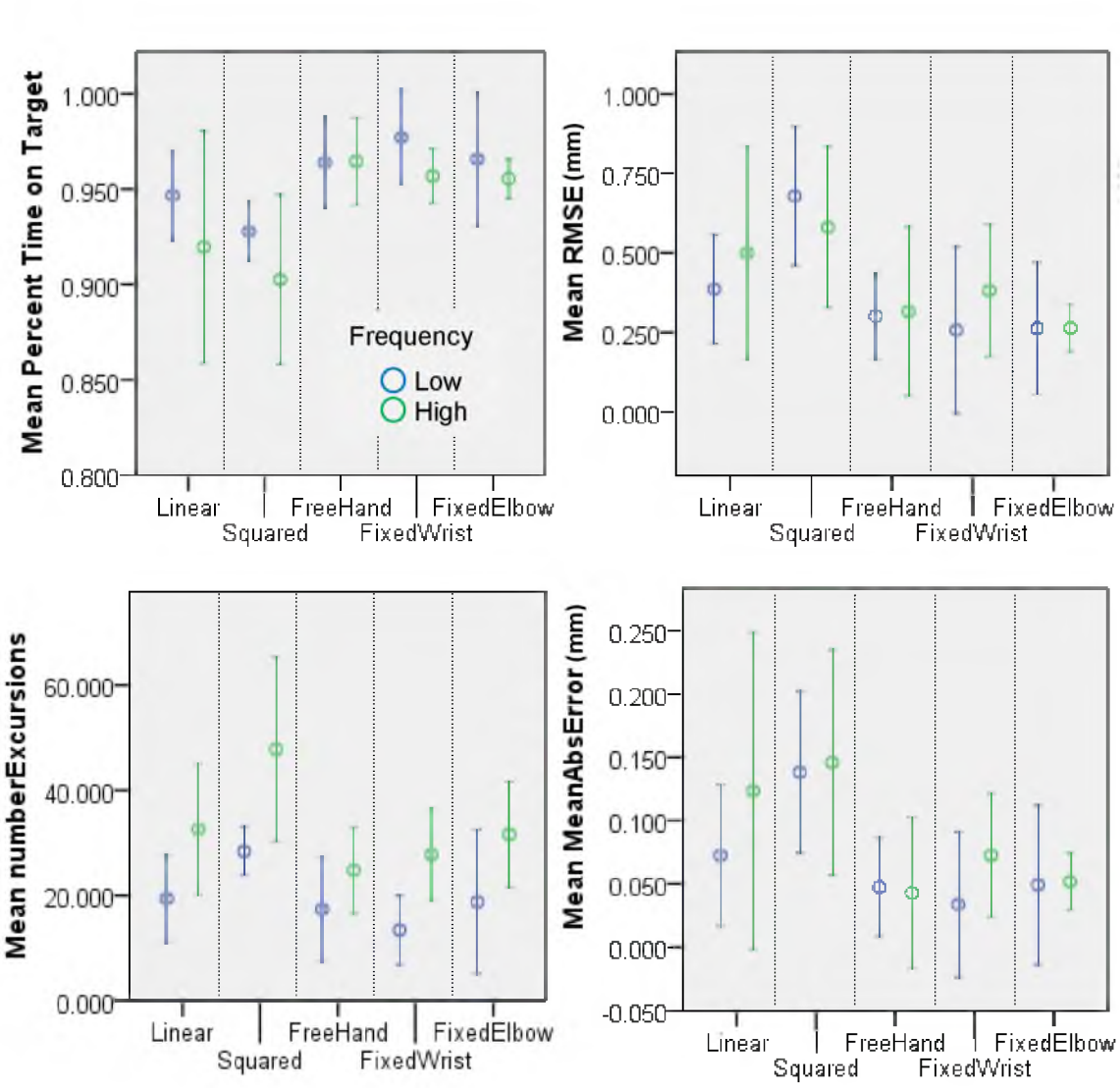

Figure 5.8 Mean and 95% confidence interval of accuracy ratings for the pilot study for all four evaluation metrics, separated by frequency. For each support condition low frequency ratings are shown on the left (in blue) and high frequency on the right (in green). For the percent time on target 1.0 correlates to 100 %. Between subjects variance has been removed from these data [30].

elbow rest to be easiest to operate while they thought that the VAHR squared admittance controller made it harder to maneuver through the path ($p < 0.005$) (Figure 5.9 right). The question concerning user fatigue shows no significant perceived difference in the fatigue experienced between support conditions (Figure 5.10).

Based on the relatively poor performance of the force input admittance controllers tested in the pilot study an experiment testing admittance control modes based on stylus position input was proposed, with the supposition that poor performance in force-based admittance modes can be attributed to the required activation of large muscle groups in the arm and shoulder. These large muscle groups are likely poorly suited to provide force input to the VAHR's instrumented armrest for the agile tracking task. Position control utilizing inputs from smaller, more dexterous inputs of the hand and fingers should prove more successful, as these inputs allow the user to control the motion of their entire arm by simply adjusting the position of their hand, avoiding the need to activate muscles controlling the shoulder and arm.

5.6 Main Experiment Results and Discussion

The main experiment included 14 participants (5 female), ages 19 to 31, two of which were left hand dominant by self report. Seven support conditions were tested in the main experiment. These support conditions were freehand, fixed elbow rest, stylus position control (Eqn. (4.4)) with three different virtual spring constants, an elastic controller (the same as Eqn. (4.4) with the addition of a spring force rendered through the Omni to the participant), and a hybrid controller using both force and stylus inputs (Eqn. (4.5)). All VAHR support conditions use the arm configuration shown in the top left of Figure 5.5. The three admittance control modes based purely on stylus position utilized virtual spring

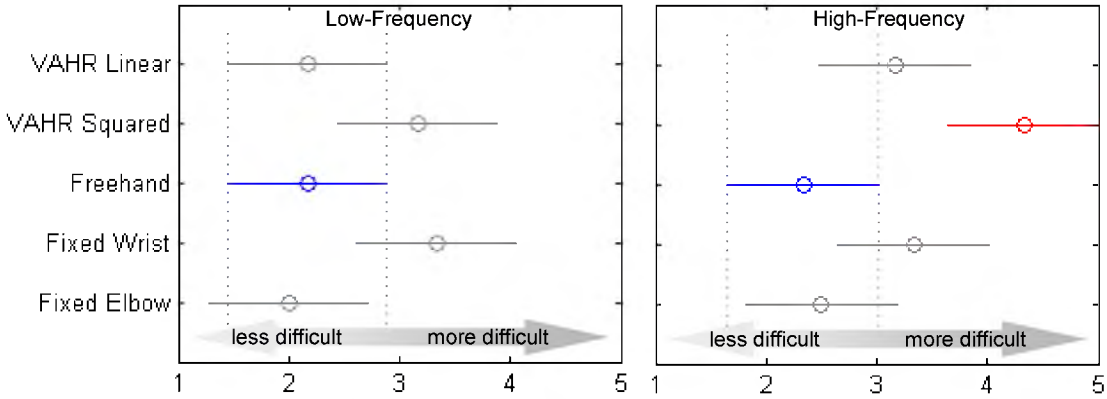

Figure 5.9 Results of Tukey's HSD for the pilot test questionnaire responses concerning the difficulty of tracking low-frequency paths (left) and high-frequency paths (right) under the various support conditions. For the right graph, the group that does not overlap either dotted line (shown in red) has a significantly different mean than the one between the two dotted lines (shown in blue).

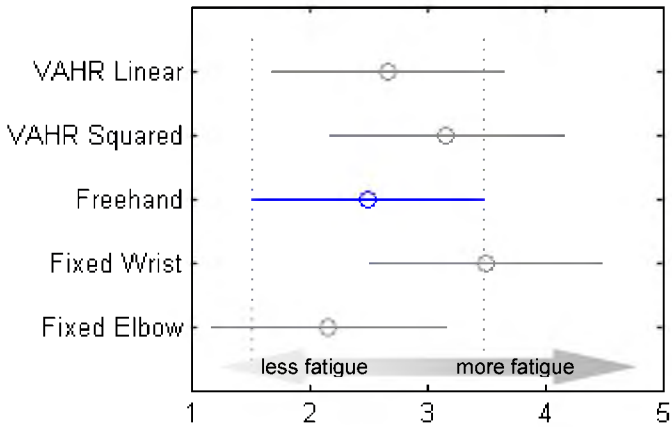

Figure 5.10 Results of Tukey's HSD for the pilot test questionnaire responses concerning the perceived fatigue under the various support conditions. No significant differences are shown.

constants of K_s = 0.222 N/mm, K_s = 0.445 N/mm, and K_s = 0.667 N/mm in combination with the directional admittance gains specified in Section 4.1.2. The elastic rate control mode used a virtual spring constant of K_s = 0.445 N/mm, to match the middle value of the pure position input controller, and a return spring force of 0.18 N/mm rendered on the stylus. The last support condition was the hybrid control law of Eqn. (4.5) with the fraction of force input set as $f_f = 0.9$ and the fraction of the position input set as $f_s = 0.5$. This results in an admittance controller that is nearly identical to the linear force input controller of the pilot study, which performed poorly relative to non-VAHR support conditions, in terms of its response to force on the support plate. The difference between the hybrid control law and the linear force input controller of the pilot study is that the hybrid control law considers input from the stylus position in addition to the force on the support plate. Thus, it is assumed that any improvements in tracking performance achieved using the hybrid controller over the linear force-based controller are a direct result of the superposition of the stylus position input.

Freehand and fixed elbow support conditions were included for comparison to the VAHR as they are good baseline conditions as to how dexterous tasks are completed without dynamic support. These two support conditions had the best accuracy ratings for RMS error and mean absolute error in the pilot test.

In the main experiment, instead of using a different set of low- and high-frequency paths for each support condition, one low-frequency path and one high-frequency path were selected and used for every support condition, removing any nonuniformity between paths. Assuming that participants had ample time to anticipate upcoming fluctuations in the path as it scrolled across the screen there would be no benefit in having prior

knowledge of the path, permitting the use of the same two paths for every support condition. Participants also completed a questionnaire for the main experiment similar to the one for the pilot study (Figure 5.6).

Box plots showing the accuracy ratings for all evaluation metrics for each support condition for both high- and low-frequency paths for the main experiment are given in Figure 5.11. Similar to the results from the pilot study tracking performance data for

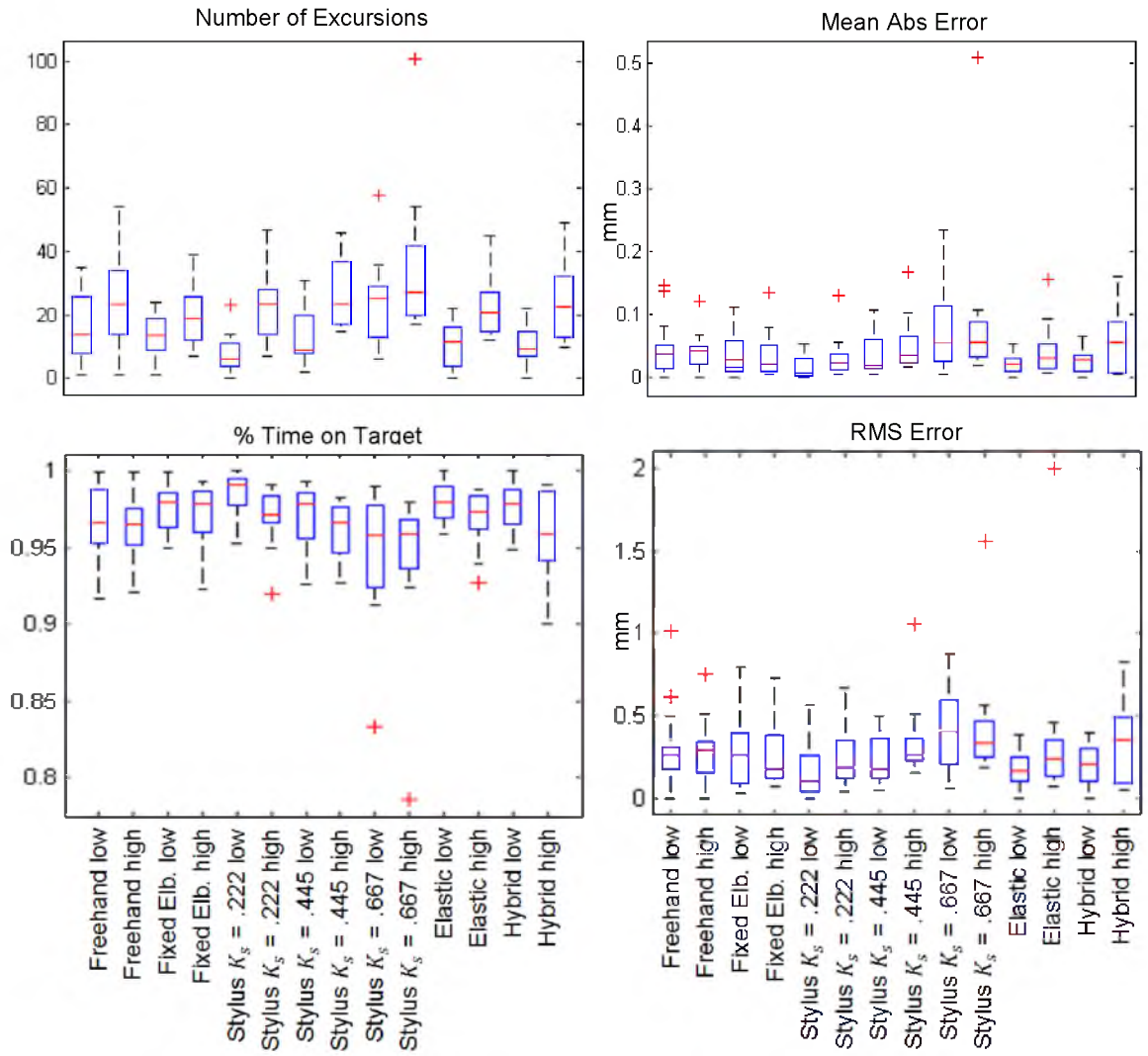

Figure 5.11 Box plots for number of excursions(top left), mean absolute error (top right), percent time on target (bottom left) and RMS error (bottom right) showing high and low frequency tracking performance for each support condition in the main experiment. For percent time on target 1 correlates to 100 %.

many of the support conditions are not normally distributed, but as mentioned previously ANOVA has been shown to be robust against violations of normality [32]. The interquartile ranges of many of the boxes corresponding with VAHR conditions more closely match those of the freehand and fixed elbow cases as compared to the results of the pilot study shown in Figure 5.7. This may indicate more consistent performance between participants, and is likely due, in part, to the greater number of participants tested in the main experiment than in the pilot study. There are more outlier points for the experiment data, so perhaps some of the data points in the pilot study that were within the interquartile range would have been classified as outliers given a group of test participants that was more representative of the general population. If this is the case the large range between the 25^{th} and 75^{th} percentiles for some of the support conditions of the pilot study makes sense.

The repeated-measures ANOVA analysis described in Section 5.4 rejects the null hypothesis that support condition has no effect on tracking performance for three of the four evaluation metrics: percent time on target [$F(2.17, 28.2) = 5.49$, $p = 0.008$] (chi-square(20) = 49.0, $p < 0.001$; $\varepsilon = 0.362$), number of excursions [$F(2.88, 37.4) = 5.07$, $p = 0.005$] (chi-square(20) = 41.6, $p = 0.004$; $\varepsilon = 0.480$), and mean absolute error [$F(1.96, 25.44) = 3.66$, $p = 0.041$] (chi-square(20) = 58.2, $p < 0.001$; $\varepsilon = 0.326$). Note that the data for these three evaluation metrics violate Mauchly's sphericity criterion so the degrees of freedom are adjusted using the Greenhouse-Geisser method (Mauchly's test results and the Greenhouse-Geisser ε are shown in parenthesis for each of these metrics in the previous sentence). The repeated-measures ANOVA does not reject the null hypothesis that the RMS error is the same between support conditions, [$F(6,78) = 2.09$, p

= 0.0641]. The p-value here is near the 0.05 level of significance, however, and if the experiment was repeated with more participants it is likely that significance would be shown for the analysis on RMS error. One other result that falls out of the ANOVA is that path frequency had a significant effect on tracking performance; [$F(1,78) > 6.93$, $p < 0.021$] for all evaluation metrics. In general, participants had better tracking performance for low-frequency paths. This supports the statement of Jagacinski and Flach that paths with more bends and tighter bends will be more difficult to track [27].

Figure 5.12 shows the mean and 95% confidence interval of participants accuracy ratings for each of the four evaluation metrics with the between subjects variance removed as in Figure 5.8 [30]. Visual comparison of the groups in the figure gives an idea of which differences might be found to be significant according to Fisher's LSD. The results of Fisher's LSD test show which support conditions had significantly different performance than the others at the $\alpha = 0.05$ level. Because the ANOVA on RMS error shows no significance for the support condition factor no further analysis is carried out using this evaluation metric.

The results of Fisher's LSD show that participants are significantly more accurate in terms of percent time on target, number of excursions, and mean absolute error for the stylus input mode with K_S = 0.222 N/mm than with no support (freehand) ($p \leq 0.035$). The stylus input mode with K_S = 0.222 N/mm also yielded significantly higher tracking accuracy than both other stylus input modes (K_S = 0.445 N/mm and K_S = 0.667 N/mm) according to all four evaluation metrics ($p \leq 0.043$). The stylus input mode with K_S = 0.667 N/mm yielded significantly less time on target than many of the other support conditions. This is the condition in which the VAHR's motion was most responsive to

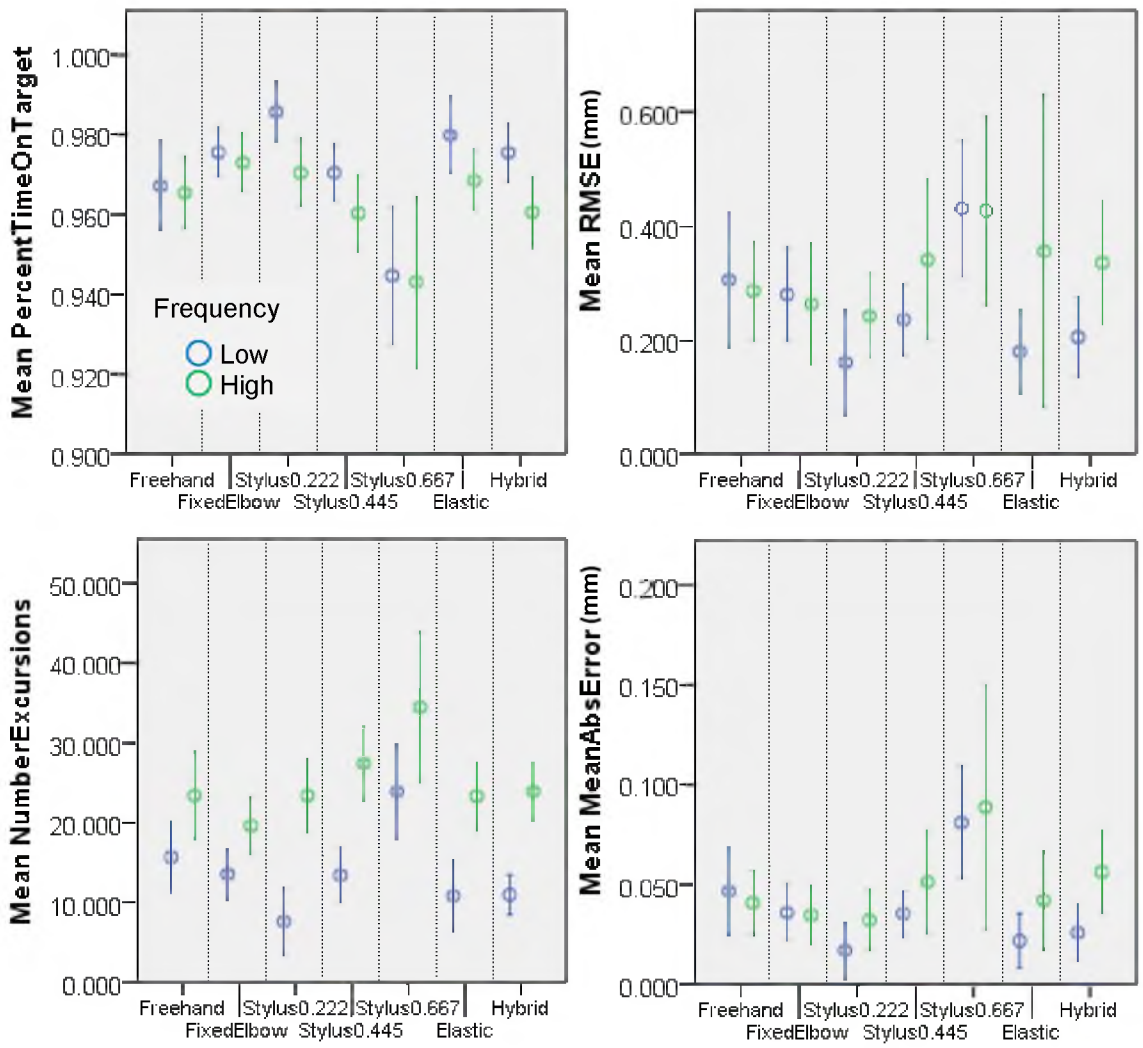

Figure 5.12 Mean and 95% confidence interval of accuracy ratings for all four evaluation metrics, separated by frequency. For each support condition low frequency ratings are shown on the left (in blue) and high frequency on the right (in green). For the percent time on target 1.0 correlates to 100 %. Between subjects variance has been removed from these data [30].

stylus motions. The P-values resulting from Fisher's LSD for all pair-wise comparisons between stylus control modes with K_s = 0.222 N/mm and K_s = 0.2667 N/mm and all other support conditions are shown in Table 5.1.

In addition to the statistical differences it is interesting to note that, for all evaluation metrics, the stylus position input mode with the lowest spring constant had the highest accuracy, outperforming both freehand and fixed elbow support conditions. This is a

Table 5.1 P-values resulting from Fisher's LSD for selected pair-wise comparisons. Significant results are highlighted in yellow

	Stylus .222 N/mm				Stylus .667 N/mm			
	% T	RMSE	# Exc	Abs E	% T	RMSE	# Exc	Abs E
Freehand	0.008	0.052	0.035	0.009	0.086	0.14	0.062	0.122
Fix. Elbow	0.463	0.197	0.632	0.277	0.006	0.027	0.005	0.028
Stylus .222	x	x	x	x	0.008	0.007	0.008	0.023
Stylus .445	0.005	0.018	0.043	0.012	0.054	0.103	0.038	0.102
Stylus .667	0.008	0.007	0.008	0.023	x	x	x	x
Elastic	0.457	0.436	0.561	0.453	0.011	0.118	0.009	0.035
Hybrid	0.081	0.192	0.42	0.084	0.027	0.038	0.004	0.069

notable improvement over the pilot study in which all of the VAHR support conditions were outperformed by all of the non-VAHR conditions. Lastly it is interesting to note that the elastic control mode had slightly better performance than stylus control with K_s = 0.445 N/mm, as these two controllers are identical with the exception that participants feel a slight return spring force pulling them towards their neutral, zero-velocity posture in the elastic control case.

Analyzing the questionnaire results for the main experiment shows a correlation between the experimental data and the participants' responses, with participants indicating that it was harder to maneuver through both low- and high-frequency paths freehand compared to the following VAHR conditions: stylus position control with K_s = 0.222 N/mm [low-frequency ($p = 0.003$), high-frequency ($p = 0.015$)], elastic control [low-frequency ($p = 0.019$), high-frequency ($p = 0.029$)], and hybrid control [low-frequency ($p = 0.001$), high-frequency ($p = 0.015$)] (Figure 5.13). Participants also perceived the freehand case to be significantly more fatiguing than all other support conditions ($p < 0.001$) with the exception of the fixed elbow rest, which was still less

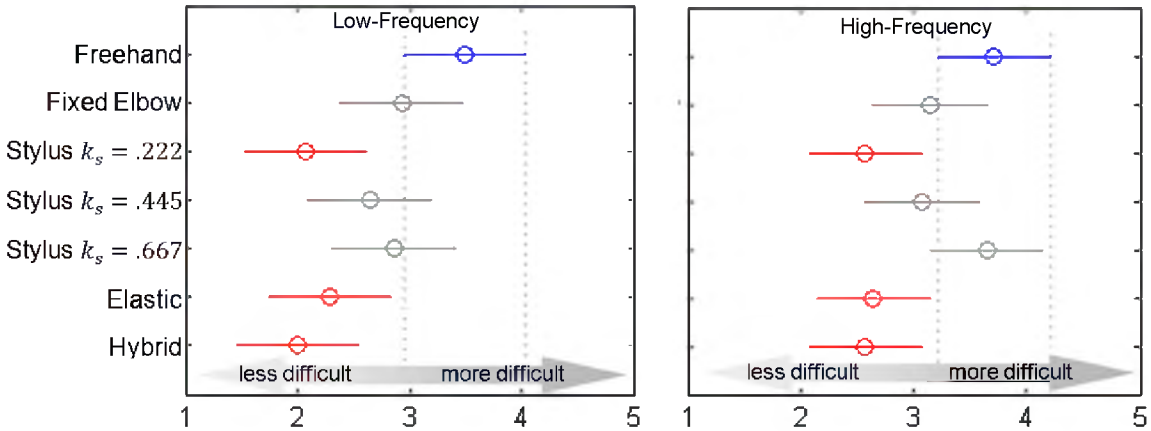

Figure 5.13 Results of Tukey's HSD for the main experiment questionnaire responses concerning the difficulty of tracking low-frequency paths (left) and high-frequency paths (right) under the various support conditions. For each graph, groups that do not overlap either dotted line (shown in red) have significantly different means than the one between the two dotted lines (shown in blue).

fatiguing but not significantly so (Figure 5.14). Test Participants found tracking to be more difficult and more fatiguing for both high- and low-frequency paths with a fixed elbow rest than with most VAHR conditions, although statistical significance is not shown for these comparisons.

Several interesting results emerge when comparing the performance of the different support conditions from both studies. Most notable is that participants performed better using the VAHR under stylus input control (K_s = 0.222 N/mm) than they did in the freehand and fixed elbow cases. This was a significant difference when comparing VAHR under stylus input control (K_s = 0.222 N/mm) to the freehand case (see Table 5.1). This supports the theory that the use of smaller, more dexterous muscle groups, such as the hand and fingers, will improve tracking performance with the VAHR. This supposition is also supported by neurobiology literature. In neurobiology a single motor neuron in combination with all of the muscle fibers that it actuates is called a motor unit. The number of muscle fibers that are innervated by a motor unit is the single motor

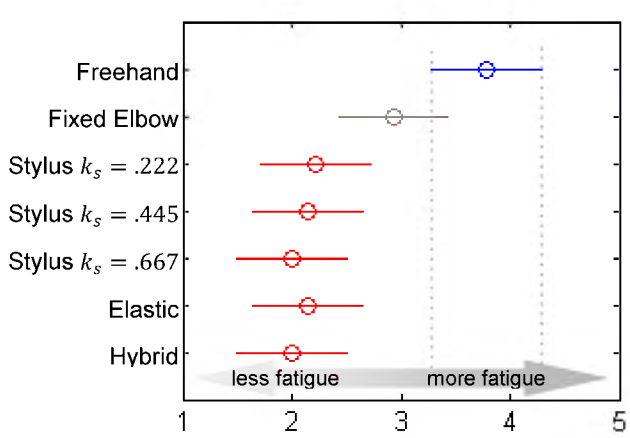

Figure 5.14 Results of Tukey's HSD for the main experiment questionnaire responses concerning the perceived fatigue under the various support conditions. Groups that do not overlap either dotted line (shown in red) have significantly different means than the one between the two dotted lines (shown in blue)

neuron's innervation ratio. Muscles that are used for precise motions are comprised of motor units with small innervations ratios, whereas muscles used for large scale coarse motions have large innervation ratios. [33] The innervation ratios of motor neurons in the hand and finger muscles are between roughly 10 and 100 [33], whereas those for neurons found in the larger arm muscles will be much larger (approximately 750 in the biceps for example [34]). Thus, it is expected that the muscles in the hand and fingers will be capable of finer control over the VAHR than those of the upper arm. Coupling participant performance in our tracking experiment with participants' reports that fatigue in the arm was reduced when using the VAHR compared to freehand and fixed elbow rest suggests that this or a similar device is capable of improving accuracy in a precise dexterous task with large workspace requirements, while also reducing muscle fatigue.

It is also interesting to note that the addition of a return spring force in the elastic control mode showed slight improvements for all evaluation metrics and in the path tracking difficulty reported by participants over the same admittance mode without the

return spring (stylus input with K_s = 0.445 N/mm). It is reasonable to assume that the stylus input control mode with the lower K_s, which already shows a significant improvement over freehand and a smaller nonsignificant improvement over fixed elbow rest, might also be improved by adding a return spring force on the stylus (i.e., implementing an elastic controller with the lower virtual spring constant of K_s = 0.222 N/mm).

Although no direct comparison is made between the pilot test results and the main experiment it is evident that both stylus input control, elastic control, and hybrid control outperform the force input modes of the pilot study. Interestingly, the linear force-based admittance mode tested in the pilot study was improved upon in relation to its performance compared to freehand and fixed elbow cases by super imposing a stylus position admittance control law (i.e., the hybrid controller condition that was tested). It is also interesting that the freehand condition, the fixed elbow rest, and both force input controllers from the pilot study are all outperformed (although not all significantly), by stylus position input control. This may suggest that control modes in which the entire arm can be repositioned without the activation of the large muscle groups in the shoulder and elbow are superior to those in which large muscle group activation is necessary (which makes sense). It may also indicate that interfacing with small muscle groups already well suited for precision manipulation in small workspaces (i.e., the wrist and fingers), will result in greater precision over the large workspace of the VAHR than can be achieved when the device takes its input from large muscle groups.

5.7 VAHR Experiment Conclusions

The results from the pilot study show that participants had lower tracking accuracy under admittance control modes in which the motion of the VAHR was controlled purely by the interaction force between the support plate and the arm/hand than for the fixed wrist and elbow conditions as well as for freehand. The poor performance of the VAHR in the pilot study led to the supposition that the large muscle groups of the shoulder and elbow, which control the motion of the VAHR in the force based admittance modes, are ill-suited to providing the control input to the VAHR for an agile tracking task. Thus, in the main experiment, several admittance control modes that use stylus position as an input were evaluated. The results for the experiment show that the VAHR under stylus control outperforms both freehand and fixed elbow support conditions, supporting the proposition that the small muscle groups of the hand and wrist, which are already tuned for precise dexterous tasks, are more apt at providing the control input to the VAHR than the large muscle groups of the arm and shoulder. An additional support linkage was designed (described in detail in the next chapter) in order to take advantage of the ability of the wrist and hand in controlling precise motion without making it necessary to track the position of the stylus. The goal of this linkage is to support the bulk of the arm and allow the wrist to control the force applied to the support plate and thus the motion of the VAHR in a force based admittance mode.

After the pilot study and the initial experiment were completed some electrical interference on the force sensor signal was detected. This interference may have been present during the pilot study and the main experiment, and could have affected participants' tracking performance with force based admittance control modes. The

extent to which the interference may have affected the test results is unknown. In light of this, at least one of the admittance modes based purely on the interaction force of the participant with the support plate should be retested in a later experiment.

CHAPTER 6

CONCLUSIONS AND ONGOING WORK

This thesis presents the design and initial evaluation of the Vertical Active Handrest, a device designed to assist the user with dexterous manipulation tasks by providing dynamic support to the arm and hand over a single vertical axis, potentially increasing the hand's precision workspace. Once the challenges of providing dynamic support on an axis aligned with gravity are well understood, the concepts of the VAHR will be integrated with those of a planar Active Handrest to create a device that provides dynamic support in a three DOF workspace. The VAHR is potentially applicable as an upper extremity rehabilitation therapy aid or as an assistive device for persons with musculoskeletal disorders such as Cerebral Palsy and Spinal Muscular Atrophy, as well as to generic tasks where precise dexterous manipulation is required.

A vertical axis tracking task was designed to evaluate the effectiveness of the VAHR under various control modes at increasing precision in a dexterous task. The VAHR was tested against static arm support conditions and against an unsupported condition, comparing the tracking accuracy under each support condition. In the pilot study two admittance control modes in which the motion of the VAHR was determined entirely by the force applied by participants to the support plate were tested and compared against fixed wrist rest, fixed elbow rest, and unsupported conditions. The tracking accuracy with the VAHR under these two force input admittance modes was worse than in the

unsupported and fixed (wrist and elbow) support cases. In the main experiment several admittance control modes in which the motion of the VAHR was determined entirely by the position of the stylus relative to the support plate and one hybrid mode that took into account both force and stylus position were compared to the freehand and fixed elbow rest conditions. The VAHR had significantly better performance than the unsupported case and better performance (though not statistically significant) than the fixed elbow case when its motion was determined by stylus input relative to the device's support plate. It is theorized that the difference in performance between the stylus input control modes of the main experiment and the force-based admittance modes of the pilot study is because the small muscle groups of the wrist and fingers are able to control the position of the entire arm in the stylus input controller, whereas it is large muscle groups of the arm and shoulder that are activated in the force input controller. This is supported by neurobiology literature on muscle motor units and innervation ratios. The small muscle groups of the hand are already adept at precise control, where the large muscle groups of the arm and shoulder are not. In order to take advantage of the aptitude of the small muscle groups of the hand at precise control an arm support linkage (presented in the next section) has been designed and mounted to the VAHR with the goal of decoupling the bulk of the arm from the force sensor input, allowing the wrist to control the force input while the weight of the entire arm is still supported against gravity.

The main contributions of the research presented in this thesis are threefold:

1. This research is the initial step in extending the concept of the Active Handrest presented by Fehlberg et al. [8] to include the vertical axis, the eventual goal of this research being a 3DOF assistive robotic device that provides support for

dexterous tasks over a large workspace. In addition to supporting and steadying the arm and hand of a healthy person for a precise dexterous task, this device could be useful in assisting disabled persons with Activities of Daily Living and in supporting upper extremity rehabilitation of patients with damaged nervous systems.

2. Various strategies for controlling the motion of the Vertical Active Handrest have been evaluated using a one DOF vertical tracking task, giving insight in how to most effectively interface with the user. The results of experimentation show that admittance control modes that set the motion of the VAHR based on the position of the stylus (or tool) relative to the support plate achieve greater tracking accuracy than admittance control modes that are based on force input provided by the muscles in the shoulder and arm. This suggests that the small muscle groups in the wrist and hand are better suited to control the motion of the VAHR than the large muscle groups of the shoulder and arm. In other words, by interfacing with muscle groups that are already tuned for small scale precise motions greater accuracy can be achieved over the workspace of the VAHR.
3. The results of the main experiment show that it is possible to achieve greater precision in a tracking task using an active support device than with no support or with a fixed elbow support. This motivates the future work on the VAHR, in order to optimize this improvement over freehand and fixed support cases.

6.1 Follower Linkage for Additional Arm Support

Although the stylus input admittance control modes had better accuracy than the force admittance modes tested it is not always convenient to track the motion of the tool in

precision manipulation tasks, which is required for stylus position input. In light of this it is desirable to develop an admittance mode that performs on par with the stylus input controller without needing to track the position of the stylus. An additional support mechanism was proposed along these lines, and under the theory that people can achieve greater precision over the workspace of the VAHR using a control mode that takes its input from the small muscle groups of the wrist and fingers, which are already geared towards precision manipulation in a small workspace. The idea behind the additional support mechanism is that the bulk of the arm can be offloaded to a separate, nonsensed support, decoupling the input to the force sensor and the task of supporting the arm against gravity, allowing the smaller, more precisely controlled muscles in the hand and wrist to provide the control input to the VAHR. After it was designed the additional arm support was manufactured and implemented (Figure 6.1). The support mechanism consists of two links that are connected by a heavy duty door hinge. The bottom link has an adjustable length and is hinged to the aluminum base of the VAHR with another heavy duty door hinge. The top link is hinged to the force sensor housing, and mounted to it is a padded trough shaped support that cradles the user's arm. This support can be repositioned to support the arm anywhere between the elbow and just below the wrist. As the VAHR translates up and down the linkage repositions the arm support to match the natural angle of the user's arm. The adjustability of the arm support linkage was designed in because the configuration that will be most beneficial to the user is still in question. Also the lower link may need to be adjusted for users of varying height and arm length.

The upper link is connected to the force sensor assembly with a custom quick release hinge (Figure 6.2). This will allow the arm support linkage to be quickly disconnected

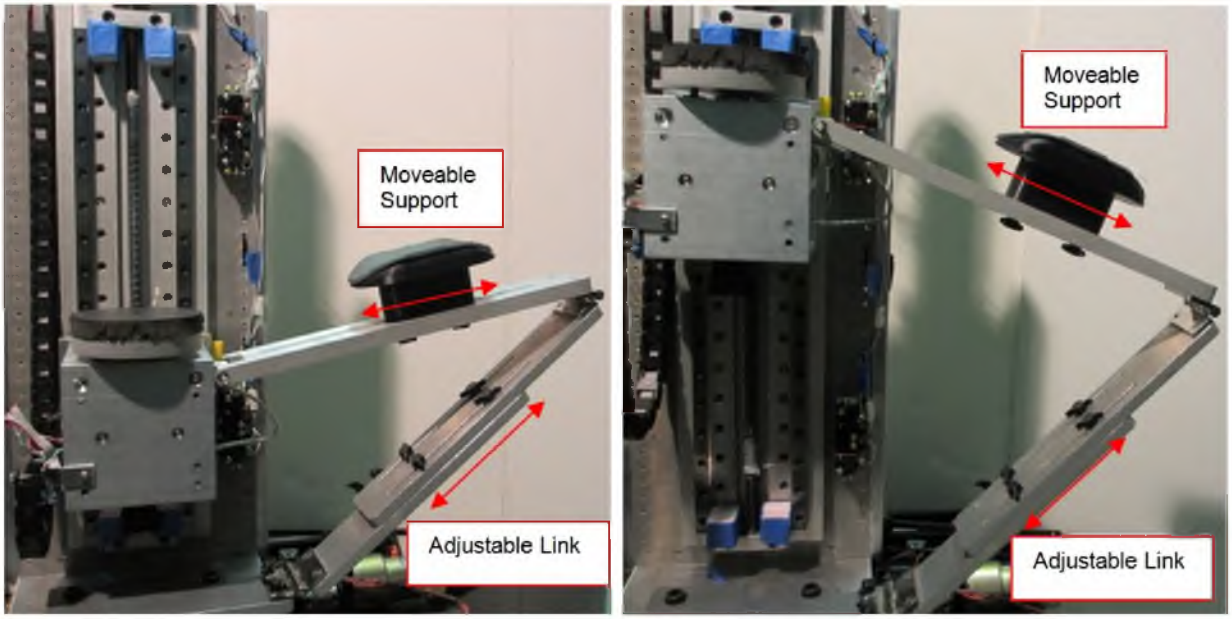

Figure 6.1 Arm Support Linkage added to VAHR, shown with the VAHR in its lowest (left) and highest (right) positions.

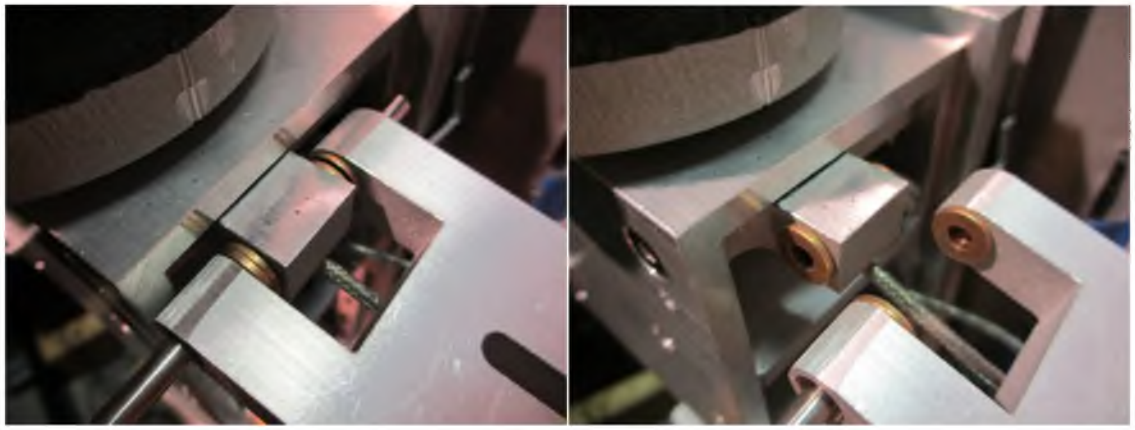

Figure 6.2 Quick release hinge connecting arm support linkage to force sensor housing. Shown connected (left) and disconnected (right).

and reconnected during experimentation in order to compare different support conditions with and without the additional support.

When operating the VAHR with the arm support linkage the user rests his/her arm on the repositionable support on the upper link, and the hand on the support plate, such that the force applied to the force sensor can be altered simply by making minor adjustments at the wrist,taking advantage of the wrist's proficiency at accomplishing small-scale precise motions. Using an admittance control mode that is based entirely on the force applied by the wrist/hand on the support plate may yield greater tracking precision than the force based admittance modes of the pilot study, and hopefully performance that is on par with the best case stylus input mode of the main experiment. No formal experimentation has been done on the VAHR with the arm support linkage, but the process of tuning gains and making alterations to the linear force based admittance control law in order to optimize the performance of the VAHR with the additional support linkage is underway.

6.2 Considerations for the Future

Based on the current progress of the Vertical Active Handrest project there are several obvious next steps to be taken. Some of these possible next steps are summarized below.

Once an acceptable admittance control mode for the VAHR with the arm support linkage (see Section 6.1) has been implemented an experiment that compares this support condition with those tested in the previous experiments should be carried out.

Given the experience of running a pilot study and an experiment there are several possible changes that might be made to the experiment architecture to yield stronger results. Although a large number of data points are gathered for each trial (i.e., one trial

equals tracking either a high or low-frequency path with a given support condition) they are all used to give a single accuracy rating for that trial. Thus, there is only one accuracy rating (for each evaluation metric) per test participant for each support condition and path frequency combination, giving a relatively small set of data for statistical analysis. Although within subjects test design and analysis helps to increase the power and promote significance with small data sets [35] it would likely be beneficial to analyze a larger data set. A larger data set could be achieved using the same number of participants by having each participant complete several repetitions of each support condition and path frequency combination while shortening the time for each trial (currently set at 2 min.) to achieve a similar overall experiment time. This would give one path accuracy rating per repetition per test participant for each support condition and path frequency combination.

There are several alterations that could be made to the tracking task that might lead to more telling results. A path that was a single sinusoidal curve (i.e., an infinitely narrow path) could be used rather than a path with two boundaries separated by a finite distance. This would eliminate the somewhat arbitrary decision of path width, and would yield a nonzero error distance for nearly every point along the path (i.e., the cursor would almost never be exactly on the path). In this case the number of excursions and percent time on target evaluation metrics would not be used. Another possible change is to display only a single dot that travels up and down to remain on the scrolling path (which would not be displayed on the monitor) and instruct participants to keep the cursor on the vertically moving dot. This would not allow test participants to plan upcoming motions ahead of time.

Experiments might also benefit by more tightly controlling the practice period before experiments begin. For the pilot study and the first experiment participants regulated their own practice period and decided when they felt comfortable with the device and the task, however, not all test participants had the same standards for "comfortableness." Implementing a training session in which each participant had to achieve a certain level of performance before being allowed to move on could help regulate the level of experience of participants coming in to the experiment.

As mentioned previously, the performance of the force-based admittance control modes tested in the pilot study may have been affected by some electrical interference that was impacting the force sensor reading. The sources of the electrical interference were twofold. First, the shielding on the force sensor cable was coming into contact with the aluminum housing of the support plate assembly, causing a small voltage jump in the force reading each time the motor moved, as the aluminum housing was picking up noise from the motor. Better isolation of the shielding solved this problem (i.e., it was electrically isolated from the VAHR's frame and force sensor enclosure). Second, the VAHR operates in the vicinity of a wire EDM machine, which is notorious for producing considerably large amplitude noise in the 1 kHz range that is picked up by the wires running to and from the motor and force sensor, as well as by the aluminum frame of the VAHR itself. The impact of this noise has been reduced by ensuring that the force sensor is properly isolated from its housing, running a ground line to the aluminum housing, and moving the VAHR as far as possible (within the available lab space) from the EDM machine. The electrical interference was not discovered until after the pilot study was completed, and whether the interference was present during the pilot study is unknown.

In light of this, it would be good to retest at least the linear force input admittance mode in the upcoming experiment. Switching to a more sensitive force sensor (e.g., the 111 or 44.5 N version of the same Omega force sensor rather than the 222 N capacity sensor that was used) and calibrating it to operate only in the range of typical user inputs would also likely improve the quality of force sensor data.

APPENDIX

DETAILS OF INITIAL PROTOTYPE EVALUATION

This appendix gives the details of the evaluation of the initial Vertical Active Handrest prototype, shown in Figure 3.4.

The stick slip behavior of the initial prototype was examined by commanding a constant velocity to the stage watching the resulting stage motion. The stick slip friction in the initial prototype is believed to be due to the interaction between the slide bearings of the linear stage with their guides. Plots illustrating the device's stick-slip behavior are shown for desired velocities of 1 and 20 mm/sec in Figure A.1. Although the magnitude of the position error was larger at higher speeds, the interference of stick-slip friction was most perceptible at low speeds. This is because the error relative to the distance traveled in a given amount of time was much higher at lower speeds than at higher ones.

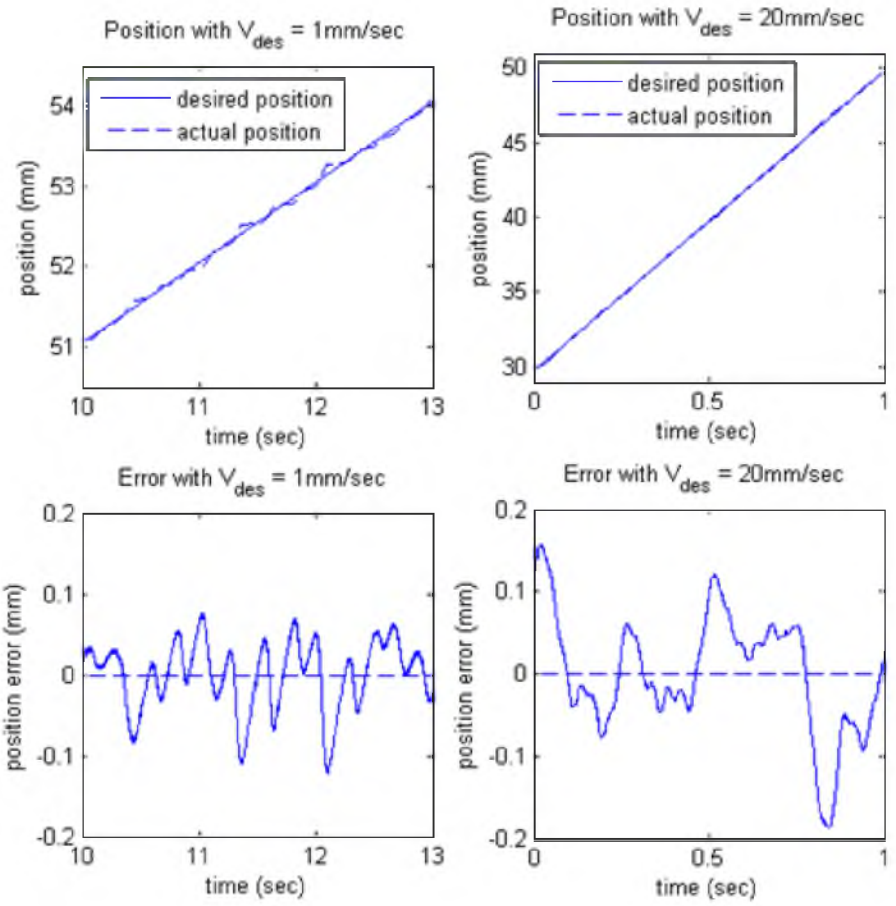

Figure A.1 The stick-slip behavior caused by the bearing.

The maximum force output the prototype was capable of applying at the interaction point between the user and the support plate was measured three different ways. First, the padded disc that would support the forearm was removed and the stage was slowly driven upward into a static surface such that all the force was transmitted directly through the rod to the force sensor. The stage was driven upward until the current to the motor had reached its maximum allowable value (dictated by software limits of ±7 V for the voltage output to the PWM amplifier) and the stage could not move up any further. Second, the VAHR prototype was programmed to track a target velocity and loaded with progressively larger test weights until it could no longer lift the weight. Third, the prototype was programmed to maintain a static desired position while increasing force was applied (by hand) to the arm support plate. The applied force was increased until the hand rest gave way under the force. Both the test weight method and the approach in which the VAHR was driven into a static surface gave similar results for the output force capability of the prototype, showing that the device was not capable of lifting loads higher than approximately 20 N. Plots showing results from the trials with 18 and 20 N test weights are shown in Figures A.2 and A.3.

The test in which the prototype was forced to deviate from a static target position showed that the device was capable of maintaining its current position under a significantly higher load than it was capable of lifting. Figure A.4 shows that the initial prototype was able to maintain a static target position to within 0.1mm until the force applied to the arm support plate reached approximately 70 N.

It is theorized that the large discrepancy between the load that the prototype was able to lift, and that which it was able to support statically was due to stick-slip friction

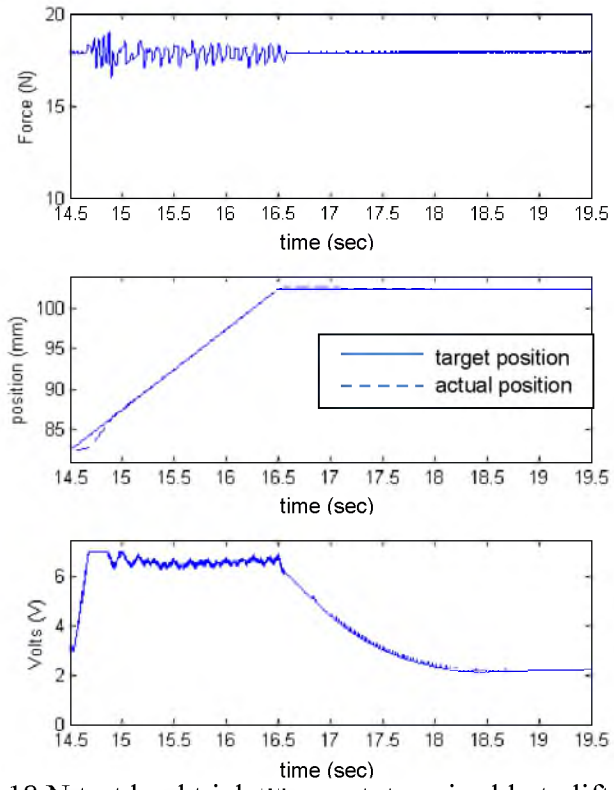

Figure A.2 18 N test load trial. The prototype is able to lift the 18 N load.

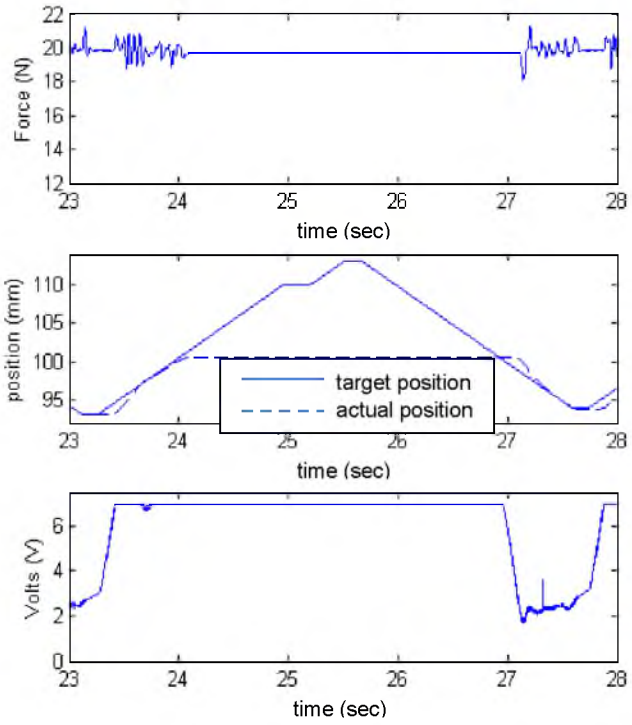

Figure A.3 20 test load trial. The prototype is not able to lift the 20 N load.

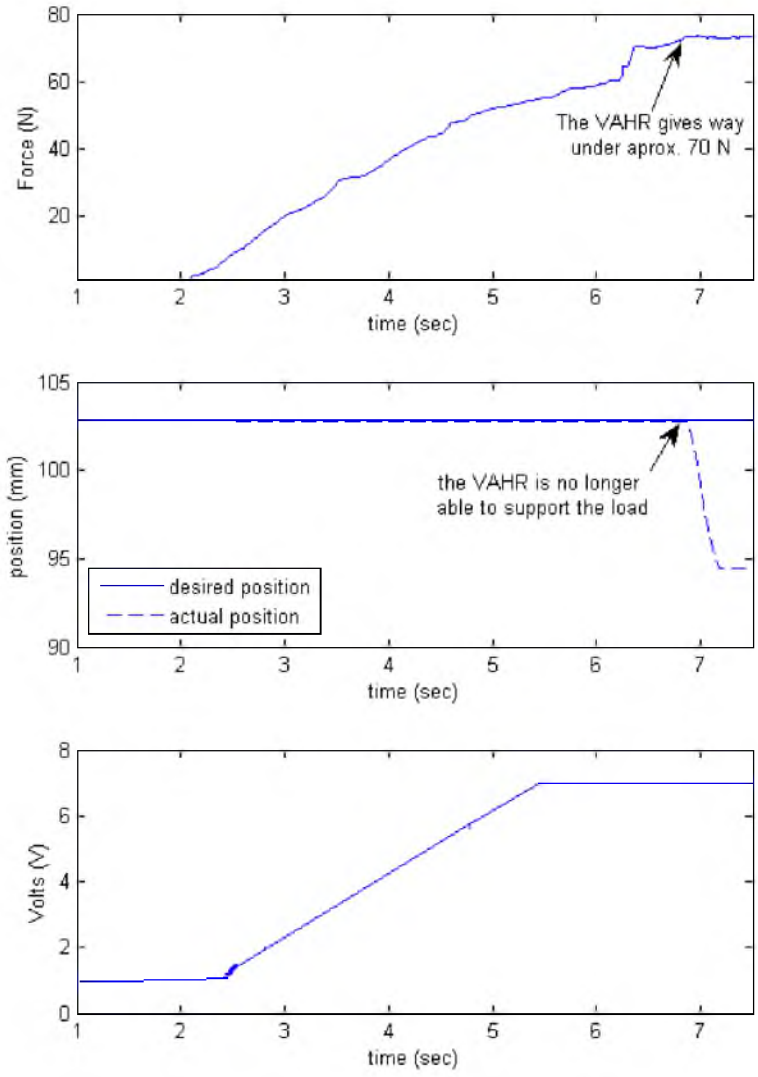

Figure A.4 The VAHR prototype is forced to deviate from its target position; it gives way under approximately 70 N.

between the rails and slide bearings of the linear stage, and to the friction in the belt drive. In the case of maintaining the current position, friction would aid the motor in supporting the load, while in the case of lifting a load friction would hinder the effort of the motor. These results proved to be problematic for users with larger arms: in some cases the force applied to the support plate was less than the threshold required to yield an upward target velocity but the motor was unable to supply the necessary torque to lift

the arm. Thus the arm would remain supported in its current position while the integrator term of a PID controller kept increasing as the VAHR was trying to lift the arm (see chapter 5 for controller details). This resulted in a sudden jump in position if the force the user was applying to the support plate ever dropped below the 20 N threshold the prototype could lift. Based on the limitations of the initial prototype the decision was made to build a new prototype using a higher end lead screw driven stage and to use a more powerful motor in hopes of reducing stick slip and increasing the force output capability.

REFERENCES

[1] S. Ito and Y. Yokokohji. "Maneuverability of master control devices considering the musculo-skeletal model of an operator." in *Proceedings of the World Haptics 2009 - Third Joint EuroHaptics conference and Symposium on Haptic Interfaces for Virtual Environment and Teleoperator Systems*, IEEE Computer Society, 2009, pp. 57-62.

[2] "EZ Rest Painting Handrest." Internet: http://www.jerrysartarama.com/discount-art-supplies/Painting-Supplies/Mahl-Sticks/EZ-Rest-Painting-Handrest.html, [Feb. 23, 2011].

[3] Rancho Rehabilitation Engineering Program. "Active Mobile Arm Support Project." Internet: http://www.ranchorep.org/project-3.html, 2005 [Feb. 2011].

[4] A.H.A Stienen, E.E.G. Hekman, F.C.T. Van der Helm, G.B. Prange, M.J.A. Jannink, A.M.M. Aalsma, H. Van der Kooij, "Freebal: dedicated gravity compensation for the upper extremities," presented at the 10th ICORR, Noordwijk, The Netherlands, Jun. 13-15, 2007.

[5] D. Odell, A. Barr, R. Goldberg, J. Chung, and D. Rempel. "Evaluation of a dynamic arm support for seated and standing tasks: a laboratory study of electromyography and subjective feedback." *Ergonomics*, Vol. 50, pp. 520-535, 2007.

[6] R.H. Taylor, P.S. Jensen, L.L. Whitcomb, A.C. Barnes, R. Kumar, D. Stoianovici, P. Gupta, Z. Wang, E. deJuan, and L. Kavoussi. "A steady-hand robotic syatem for microsurgical augmentation." *International Journal of Robotics Research*, Vol. 18, pp. 1201–1210, 1999.

[7] J.E. Colgate, W. Wannasuphoprasit, and M.A. Peshkin. "Cobots: robots for collaboration with human operators." in *Proceedings of ASME Dynamic Systems Control Division,* Vol. DSC-58, pp. 433-440, 1996.

[8] M.A. Fehlberg, B.T. Gleeson, L.C. Leishman, W.R. Provancher, "Active Handrest for Precision Manipulation and Ergonomic Support." in *Proceedings of the Symposium on Haptic Interfaces for Virtual Environments and Teleoperator Systems*, 2010, pp. 25-26.

[9] M.A. Fehlberg, B.T. Gleeson, and W.R. Provancher, "Active Handrest: a large workspace tool for precision manipulation." *International Journal of Robotics Research*, Vol. 31, pp. 289-301, Mar. 2012.

[10] "Dynamic Arm Supports of ARMON." Internet: www.armonproducts.com, [Nov. 2011].

[11] J.L. Herder. "Development of a statically balanced arm support: ARMON," in *Proceedings of the IEEE 9th International Conference on Rehabilitation Robotics*, 2005, pp. 281-286.

[12] G. Kramer, G.R.B.E. Romer, and H.J.A. Stuyt. "Design of a Dynamic Arm Support (DAS) for gravity compensation," in *Proceedings of the IEEE 10th International Conference on Rehabilitation Robotics*, 2007, pp. 1042-1048.

[13] "Neater Arm Support" Internet: neater.co.uk/main.htm, [Nov. 2011].

[14] R. Riener, T. Nef, G. Colombo. "Robot-Aided Neurorehabilitation of the Upper Extremities." *Medical and Biological Engineering and Computing*, Vol. 43, pp. 2-10, 2005.

[15] R. Beer, M. Ellis, B. Holubar, J. Dewald, "Impact of Gravity Loading on Post Stroke Reaching and its Relationship to Weakness." *Muscle & Nerve*, Vol. 36, pp. 242-250. Aug. 2007.

[16] R.F. Beer, C. Naujokas, B. Bachrach, D. Mayhew. "Development and Evaluation of a Gravity Compensated Training Environment for Robotic Rehabilitation of Post-Stroke Reaching," in *Proceedings of the second IEEE/RAS-EMBS International Conference on Biomedical Robotics and Biomechatronics*, 2008, pp. 205-210.

[17] H.I. Krebs, N. Hogan, M.L. Aisen, and B.T. Volpe. "Robot-Aided Neurorehabilitation." *IEEE Transactions on Rehabilitation Engineering*, Vol. 6, pp. 75-87, Aug 2002.

[18] R. Loureiro, F. Amirabdollahian, M. Topping, B. Driessen, and W. Harwin. "Upper Limb Robot Mediated Stroke Therapy-GENTLE/s Approach." *Autonomous Robots,* Vol. 15, pp. 35-51, Jul 2003.

[19] C.E. Clauser, J.T. McConville, and J.M. Young. "Weight, Volume, and Center of Mass of Segments of the Human Body." Technical Report AMRL-TR-69-70, Aerospace Medical Research Laboratory, Wright-Patterson Air Force Base, Dayton, OH. pp.42-45, Aug 1969

[20] Omega Engineering inc. "Load Cells, Force Sensors and Torque Transducers." Internet: http://www.omega.com/toc_asp/subsectionSC.asp?subsection=f&book=Pressure&all=1, [Feb. 3, 2011].

[21] Servo Systems CO. "Low Profile Series Linear Stages – Model LPS 12-20." Internet: http://www.servosystems.com/lps_12-20.pdf, [Dec. 16, 2011].

[22] Servo Systems CO. "Electrocraft Brush Type Dc Servo Motor Specifications." Internet: http://www.servosystems.com/electrocraft_dcbrush_rdm103.htm, [Dec. 16, 2011].

[23] F. Conti, F. Barbagli, D. Morris, and C. Sewell. "CHAI 3D: An Open-Source Library for the Rapid Development of Haptic Scenes," presented at the IEEE World Haptics Conference, Pisa, Italy, March 18-20, 2005.

[24] S. Zhai. "Investigation of Feel for 6 DOF Inputs: Isometric and Elastic Rate Control for Manipulation in 3D Environments," in *Proceedings of the Human Factors and Ergonomics Society 37th Annual Meeting*, Oct. 1993, pp. 323-327.

[25] P.M. Fitts. "The information capacity of the human motor system in controlling the amplitude of movement." *Journal of Experimental Psychology*, Vol. 47, pp. 381–391, June 1954.

[26] D.A. Kontarinis, R.D. Howe, and P. Hall. "Tactile Display of Vibratory Information in Teleoperation and Virtual Environments." *Applied Sciences*, Vol. 4, pp. 387-402, 1995.

[27] R.J. Jagacinski, and J.M. Flach. *Control Theory for Humans: Quantitative Approaches to Modeling Performance*. Mahwah, New Jersey, Lawrence Erlbaum Associates, 2003, pp. 104-111.

[28] D. Morris, H. Tan, F. Barbagli, T. Chang, and K. Salisbury. "Haptic Feedback Enhances Force Skill Learning," in *Proceedings of the World Haptics 2007 - Second Joint EuroHaptics Conference and Symposium on Haptic Interfaces for Virtual Environment and Teleoperator Systems*, 2007, pp. 21-26.

[29] A. Bardorfer, M. Munih, A. Zupan, and A. Primozic, "Upper Limb Motion Analysis Using Haptic Interface." *IEEE Transactions on Mechatronics*, Vol. 6, pp. 253-260, Sep. 2001.

[30] D. Cousineau. "Confidence intervals in within subject designs: A simpler solution to Loftus and Masson's method." *Tutorials in Quantitative Methods for Psychology*, Vol. 1, pp. 42–45, 2005.

[31] H.J. Keselman. "Testing treatment effects in repeated measures designs: An update for psychophysiological researchers." *Psychophysiology*, Vol. 35, pp. 470– 478, 1998.

[32] E. Schmider, M. Ziegler, E. Danay, L. Beyer, and M. Bühner. "Is it really robust? Reinvestigating the robustness of ANOVA against violations of the normal distribution assumption." *Methodology: European Journal of Research Methods for the Behavioral and Social Sciences*, Vol. 6, pp.147-151, 2010.

[33] J. Knierim. "Motor Units and Muscle Receptors" in *Neuroscience Online.* [On-line]. Available: http://neuroscience.uth.tmc.edu/s3/chapter01.html, [Jan. 2012].

[34] M.K. Floeter. "Structure and Function of Muscle Fibers and Motor Units" in *Disorders of Voluntary Muscle.* [On-Line]. Available: http://assets.cambridge.org/97805218/76292/excerpt/9780521876292_excerpt.pdf, [Jan. 2012].

[35] H.J. Seltman. *Experimental Design and Analysis*. pp. 339-356. [On-line]. Available: www.stat.cmu.edu/~hseltman/309/Book/Book.pdf, [Nov. 2011].